Scientific Reports

https://doi.org/10.1038/s41598-026-39262-4

Article in Press

M2 macrophage–derived extracellular vesicles induce EMT-like transcriptional reprogramming in colorectal cancer cells via upregulation of FAM83A

Received: 24 August 2025

Accepted: 4 February 2026

Published online: 19 February 2026

Cite this article as: Isik M., Akkulak M. & Derkus B. M2 macrophage–derived extracellular vesicles induce EMT-like transcriptional reprogramming in colorectal cancer cells via upregulation of FAM83A. *Sci Rep* (2026). https://doi.org/10.1038/s41598-026-39262-4

Melis Isik, Merve Akkulak & Burak Derkus

We are providing an unedited version of this manuscript to give early access to its findings. Before final publication, the manuscript will undergo further editing. Please note there may be errors present which affect the content, and all legal disclaimers apply.

If this paper is publishing under a Transparent Peer Review model then Peer Review reports will publish with the final article.

ARTICLE IN PRESS

© The Author(s) 2026. **Open Access** This article is licensed under a Creative Commons Attribution-NonCommercial-NoDerivatives 4.0 International License, which permits any non-commercial use, sharing, distribution and reproduction in any medium or format, as long as you give appropriate credit to the original author(s) and the source, provide a link to the Creative Commons licence, and indicate if you modified the licensed material. You do not have permission under this licence to share adapted material derived from this article or parts of it. The images or other third party material in this article are included in the article's Creative Commons licence, unless indicated otherwise in a credit line to the material. If material is not included in the article's Creative Commons licence and your intended use is not permitted by statutory regulation or exceeds the permitted use, you will need to obtain permission directly from the copyright holder. To view a copy of this licence, visit http://creativecommons.org/licenses/by-nc-nd/4.0/.

ARTICLE IN PRESS

M2 Macrophage–Derived Extracellular Vesicles Induce EMT-Like Transcriptional Reprogramming in Colorectal Cancer Cells via Upregulation of FAM83A

Melis Isik[1], Merve Akkulak[2], Burak Derkus[1*]

1. Stem Cell Research Lab, Department of Chemistry, Faculty of Science, Ankara University, 06560 Ankara, Turkiye
2. Department of Biological Sciences, Faculty of Science, Middle East Technical University, Ankara 06800, Turkiye

*Corresponding Author: Prof. Burak Derkus, E-mail= bderkus@ankara.edu.tr

Abstract

In the complex landscape of cancer progression, the immune system shapes crucial interactions between tumor and immune cells. Understanding this dialogue is essential for elucidating how immune-derived cues trigger epithelial-mesenchymal transition (EMT)-like transcriptional changes, a fundamental process that drives tumor cell plasticity and facilitates aggressive phenotypes. Here, we investigated the crosstalk between M2 macrophages and colon cancer cells (HT-29) during the post-tumorigenic phase, focusing on exosome-mediated regulation of EMT, a critical pathway controlling tumor cell phenotypic and transcriptional dynamics. Co-culture experiments revealed that M2 macrophage–derived exosomes (M2-Exo) induced profound transcriptional changes, with downregulation of epithelial markers and increased expression of mesenchymal genes. Importantly, EMT induction was markedly stronger following M2-Exo treatment than in the co-culture setting, suggesting that while soluble mediators play a contributory role, EMT is predominantly and directly driven by exosome-mediated signaling. Transcriptomic profiling identified FAM83A as a key upregulated gene in M2-Exo–treated HT-29 cells. Functional analyses demonstrated that FAM83A promoted EMT by modulating regulators associated with decreased E-Cadherin and increased N-Cadherin, MMP2, and MMP9 expression. Importantly, siRNA-mediated silencing of FAM83A abolished its overexpression and inhibited EMT activation, confirming its essential role in M2-Exo–induced programming of EMT. Collectively, these findings highlight exosome-mediated immune-tumor interactions as critical drivers of EMT and the progression toward an invasive, mesenchymal-like phenotype.

Keywords: Extracellular Vesicles**,** Exosomes, FAM83A, Cancer, Epithelial-Mesenchymal Transition, Immune-Oncology

ARTICLE IN PRESS

1. Introduction

Cancer remains one of the most formidable challenges in human health, affecting individuals and populations across the globe. It is not a solitary entity; rather, it thrives within a complex ecosystem known as the tumor microenvironment (TME), where an intricate interplay among cellular components and signaling pathways determines tumor progression and response to therapy. Our understanding of this multifaceted relationship has significantly advanced in recent years, offering novel insights into cancer biology and informing innovative therapeutic strategies. The cancer microenvironment is a dynamic milieu, consisting of immune cells, stromal cells, blood vessels, and extracellular matrix components, all of which can influence tumor growth, invasion, and response to treatment.

At the heart of this dynamic battleground lies the immune system, a remarkable defense mechanism of the body with the potential to suppress and aid cancer progression.[1] The interaction between cancer cells and the immune system within the TME is a pivotal factor that shapes the course of the disease. Among immune cells, macrophages play a particularly prominent role, exhibiting two major phenotypes: M1 and M2. M1 macrophages, stimulated by pro-inflammatory cytokines such as TNF-α and IL-12, exert anti-tumorigenic effects by enhancing immune responses, promoting tumor cell phagocytosis, and correlating with improved prognosis and enhanced responsiveness to immunotherapies [2–4]. In contrast, M2 macrophages secrete anti-inflammatory cytokines including IL-10 and TGF-β, which create an immunosuppressive environment that facilitates tumor progression and metastasis by promoting angiogenesis, tissue remodeling, immune evasion, and therapy resistance [5–9]. These immunomodulatory effects can alter the tumor landscape in multiple ways, including suppression or enhancement of anti-tumor immunity, increased invasiveness, and remodeling of the TME to favor tumor survival. Notably, co-culture studies involving cancer cells and

ARTICLE IN PRESS

tumor-associated macrophages (TAMs) have revealed activation of specific genes and pathways, such as those involved in aerobic glycolysis, upregulation of CCL2 chemokines, and modulation of VEGF receptor expression on cancer cells [10–12].

Within the intricate landscape of cancer biology, an emerging player has garnered increasing attention -exosomes. Exosomes are nano-sized membrane-bound vesicles secreted by various cell types, including macrophages.[13] These minuscule packages are replete with proteins, lipids, nucleic acids, and bioactive molecules, all carefully packaged to facilitate intercellular communication. Exosomes, play critical roles in cancer biology, significantly influencing tumor progression, metastasis, and the tumor microenvironment.[14] In the context of cancer, exosomes facilitate communication between tumor cells and their surroundings, promoting angiogenesis, immune evasion, and pre-metastatic niche formation.[15] They can transfer oncogenic signals to recipient cells, thus modulating their behavior to support tumor growth and spread.[16] Additionally, exosomes are crucial in mediating drug resistance by facilitating the efflux of anticancer drugs and disseminating resistance-conferring molecules to surrounding cells.[17] On the other hand, the abovementioned intricate web of communication orchestrated by macrophages could be exosome-mediated.[18] Yet, the discovery of immune-triggered carcinogenic exosomal gene pathways within macrophages remains elusive, representing a significant opportunity to enhance cancer immunotherapy by transforming the tumor-promoting attributes of macrophage-derived EVs into anti-tumorigenic traits. Therefore, understanding the roles and mechanisms of macrophage exosomes in cancer biology is essential for deciphering the complexities of tumor development and devising innovative therapeutic strategies.

This study investigates the EMT-related transcriptional modulation induced by macrophage-derived exosomes, leading to the activation of dormant

ARTICLE IN PRESS

oncogenes in colorectal cancer cells. As a model, we established a co-culture model of colorectal cancer cells (HT-29) and M2 macrophage-derived exosomes (M2-Exo), enabling a platform to investigate the roles of exosomes in post-tumorigenic processes. The potential of M2-Exo to induce EMT and drive early motile phenotypes in HT-29 cells were assessed by a broad spectrum of techniques, including immunofluorescent microscopy, real-time-quantitative polymerase chain reaction (RT-qPCR), and mRNA-seq. Finally, a proto-oncogene was determined to be responsible for the initiation of EMT in colorectal cancer cells, and its validation was further carried out by using oncogene-specific siRNAs.

2. Experimental Section

2.1. Cell culture

HT-29 (ATCC® HTB-38™, kindly provided by Prof. Erkan Yilmaz, Biotechnology Institute, Ankara University, Turkey), Raw267.4 (ATCC® TIB-71™) and T98G cells (ATCC® CRL-1690™, kindly provided by Prof. Orhan Adalı, Middle East Technical University, Turkey), MCF-7 cells (ATCC® HTB-22™, kindly provided by Prof. Ahmet Acar, Middle East Technical University, Turkey), and 451LU cells (Rockland #451lu-01-0001, kindly provided by Prof. Guliz Ak Demir, Ege University, Turkey) were cultured in Dulbecco's Modified Eagle's Medium-High Glucose (DMEM-HG, Thermo Fisher, USA) supplemented with fetal bovine serum (FBS, 10% v/v, Thermo Fisher, USA) and penicillin-streptomycin (P/S, 1% v/v, Thermo Fisher, USA) in a CO_2 incubator at 37 °C and 5% CO_2 humidity conditions. The medium was refreshed every 3 days until the desired cell confluency was accomplished. For the induction of the M2 phenotype in Raw 264.7 cells, the cells were cultured in DMEM-HG supplemented with IL-10 (50 ng/mL) for 48 hours. Following the 48-hour polarization period, the medium was replaced with DMEM-HG without IL-10 and maintained in this condition for subsequent experiments. To compare the M1 phenotype and validate the success of M2

ARTICLE IN PRESS

polarization, Raw 264.7 cells were cultured in DMEM-HG supplemented with LPS (100 ng/mL) and IFN-gamma (20 ng/mL) for M1 induction. The success of polarization was evaluated by RT-qPCR analysis of markers specific for the M1 phenotype (CD64, STAT-1) and the M2 phenotype (CD163, STAT-6). Primer sequences (Oligomer Biotechnology Jsc., Turkey) are provided in the SI. Each quantitative experiment was performed with three replicates with two biological replicates. Statistical differences among groups were assessed by t-test, one-way ANOVA followed by Tukey's post hoc test.

2.2. Co-culture of M2 macrophages with HT-29 colorectal cancer cells

To investigate the crosstalk between the immune system and cancer cells, HT-29 cells and M2 macrophages were co-cultured using a two-compartment Transwell system separated by a 0.4-μm porous membrane, which allows the transfer of macrophage-derived factors (proteins, metabolites, lipids, mRNAs, miRNAs, snRNAs, etc.) into the lower chamber containing cancer cells. Initially, HT-29 cells and M2 macrophages were seeded separately into the lower and upper chambers, respectively, and cultured for 24 hours to ensure proper cell attachment. After this pre-culture period, the compartments were assembled to initiate the co-culture. To model the immune–cancer interaction, three different HT-29 to M2 macrophage ratios (1:2, 1:1, and 2:1) were established by seeding 1×10^5 M2 macrophages in the upper inserts and varying the number of HT-29 cells (5×10^4, 1×10^5, or 2×10^5) in the lower wells. The co-culture was maintained for 5 days, after which analyses were conducted. All conditions were performed in triplicate using independent Transwell setups.

2.3. Exosome isolation and characterization

Exosomes were isolated from M2 macrophages through serial ultracentrifugation according to the detailed protocol carried out in our previous studies.[19–21] Briefly, secretion-rich medium (SRM) was filtered

ARTICLE IN PRESS

by using 0.22-μm filters for the elimination of unwanted cells in the SRM and gradual centrifugation was performed at 300 *g* for 10 min, 2000 *g* for 10 min, and 10,000 *g* for 30 min, respectively, for the removal of cellular residues, apoptotic bodies, and large molecular weight proteins. Finally, SRM was ultracentrifuged (Himac CP100WX, Hitachi, USA) for 90 min at 120.000 *g* to obtain an exosome pellet.

The isolated exosome pellet was resuspended in sterile PBS and characterized with several techniques. Total exosomal protein content was measured using a bicinchoninic acid (BCA) test (Thermo Fisher, USA) by recording the optic measurements of absorbances at 562 nm on a microplate reader (Thermo Scientific, Multiskan Sky Microplate Spectrophotometer). Nanoparticle tracking analysis (NTA) was carried out at 1:1000 dilution for the determination of particle size with a NanoSight LM10 instrument equipped with the NTA 2.0 analytical software. Nano-morphology of the isolated exosomes was characterized by counterstaining with uranyl acetate and visualized under transmission electron microscope (TEM, JEOL JEM 100CX II, Tokyo, Japan). For Western Blot (WB) analysis, the extracted proteins were separated by sodium dodecyl sulfate-polyacrylamide gel (SDS-PAGE) electrophoresis and, subsequently, transferred onto a polyvinylidene difluoride (PVDF) membrane. The membrane was blocked with 5% skimmed milk at room temperature for 1 h. Immunoblotting was performed with exosome-specific antibodies namely CD63 and CD81 (1:200, Santa Cruz, USA) with overnight incubation at 4 ^{o}C, followed the incubation with horseradish peroxidase (HRP)-conjugated anti-mouse IgG (1:2000, Abcam, UK) for 1 h at room temperature. Proteins were then visualized using SuperSignal West Femto electrochemiluminescence (ECL) substrate (Bio-Rad, USA).

2.4. Induction of HT-29 cells with M2-Exo

To demonstrate that macrophages influence cancer cells through an exosome-mediated mechanism, HT-29 cells were treated with M2-Exo under

ARTICLE IN PRESS

various experimental conditions. To optimize the M2-Exo–based induction protocol, we systematically evaluated the effects of initial cell density, exosome concentration, and exosome application frequency. For this purpose, a fixed concentration of M2-Exo (100 µg/mL) was applied to HT-29 cells 24 hours after seeding in 24-well plates at varying densities (5×10^4, 1×10^5, and 2×10^5 cells per well). To determine the optimal exosome concentration based on the selected cell density, HT-29 cells (5×10^4 cells per well) were treated with increasing concentrations of M2-Exo (50, 100, and 200 µg/mL). Additionally, the frequency of M2-Exo administration was optimized by exposing HT-29 cells (5×10^4 cells per well) to the optimized concentration (50 µg/mL) once, twice, or three times during the 5-day culture period. In all experiments, culture media were refreshed every 2 to 3 days in alignment with the exosome treatment schedule. Cells were maintained under standard incubation conditions (95% relative humidity, 37 °C, and 5% CO_2) for either 2 or 5 days, depending on the experimental design.

2.5. Investigation of cytocompatibility of M2 macrophages and M2-Exo

Live/Dead Assay: To assess the effects of varying M2 macrophage culture densities in co-culture with HT-29 cells, as well as the impact of different M2-Exo concentrations and application frequencies on HT-29 cell viability and proliferation, live/dead staining and XTT assays were performed prior to subsequent experiments. For visualization of HT-29 cell viability over a 5-day culture period, cells were stained with calcein-AM (4 µM; Molecular Probes, Thermo Fisher, UK) to detect live cells, and ethidium homodimer-1 (EthD-1, 2 µM; Molecular Probes, Thermo Fisher, UK) to detect dead cells. Fluorescence imaging was carried out using a Leica DMIL fluorescence microscope (Germany) at excitation/emission wavelengths of 488 nm (green) and 527 nm (red), respectively.

ARTICLE IN PRESS

Cell Proliferation Assay: To further evaluate HT-29 cell proliferation in the Transwell co-culture and M2-Exo induction experiments, XTT assays (Biological Industries, USA) were conducted. After 2 and 5 days of culture, HT-29 cells were washed and incubated with XTT working solution (1:2 ratio of XTT reagent to culture medium). Absorbance values were measured at 490 nm using a microplate spectrophotometer (Multiskan Sky, Thermo Fisher, USA) following a 2-hour incubation. All experiments were carried out in 24-well plates compatible with Transwell inserts. Each quantification assay was performed in biological triplicate. Statistical differences among multiple groups were analyzed using one-way ANOVA followed by Tukey's post hoc test.

2.6. Investigating the post-tumorigenic effects of M2 macrophages and M2-Exo through gene expression analysis

ARTICLE IN PRESS

To assess the pro-tumorigenic effects of M2 macrophages and M2-Exo on HT-29 cells and to optimize an exosome-mediated in vitro model, RT-qPCR analyses were performed targeting metastasis-related markers (*MMP-2* and *MMP-9*) as well as EMT-associated genes (*E-Cadherin* and *N-Cadherin*). As part of the gene expression analysis, alterations in the metastatic gene signature of HT-29 cells co-cultured with M2 macrophages at varying ratios (HT-29:M2 = 1:2, 1:1, 2:1) were examined. The role of M2-Exo was further investigated through a series of experiments modulating initial HT-29 cell density, M2-Exo concentration, and loading frequency, to delineate the specific contribution of exosomes to metastatic potential. At the end of the 5-day culture period, total RNA was extracted (GeneDireX, USA) and reverse-transcribed into cDNA using a commercially available kit (Bio-Rad, USA). RT-qPCR was conducted using a Bio-Rad CFX96 real-time thermal cycler (USA). Primer sequences (Oligomer Biotechnology Jsc., Turkey) are listed in the Supporting Information (**Table S1**). All quantitative RT-qPCR experiments were carried out in triplicate with three independent biological replicates.

ARTICLE IN PRESS

Statistical significance among multiple groups was assessed using one-way ANOVA followed by Tukey's post hoc test.

2.7. Examining EMT in HT-29 cells in response to M2 macrophages co-culture and M2-Exo treatment

To visualize the loss of epithelial cell polarity and the concurrent increase in mesenchymal phenotype, immunofluorescent staining was performed for the epithelial tumor suppressor protein E-cadherin and the mesenchymal tumor promoter protein N-cadherin in HT-29 cells subjected to either M2 macrophage co-culture (at the optimized cell ratio) or M2-Exo treatment. Following a 5-day culture period, HT-29 cells were fixed with 4% (v/v) paraformaldehyde (PFA; Sigma) for 15 minutes and permeabilized with 0.1% (v/v) Triton X-100 (Sigma). Non-specific binding sites were blocked by incubating the cells in 0.1% (v/v) bovine serum albumin (BSA; Sigma), followed by staining with primary antibodies against E-cadherin (1:200, Santa Cruz, USA) and N-cadherin (1:200, Santa Cruz, USA) according to the manufacturer's instructions. After overnight incubation at 4 °C, cells were washed and incubated with Alexa Fluor 488-conjugated anti-mouse secondary antibody (1:1000, Thermo Fisher, USA). Nuclear staining was performed using DAPI (Thermo Fisher, USA). E-cadherin^{+} and N-cadherin^{+} cells were visualized under a fluorescence microscope (Leica DMIL, Germany) using the green and red fluorescence channels, respectively.

2.8. Transcriptome analysis and bioinformatics

Transcriptome analysis was performed in HT-29 cells to investigate the effects of M2-Exo on mRNA level. For this purpose, a co-culture experiment was set considering the optimized parameters (HT-29:M2 macrophages=1:2; initial cell density of HT-29 cells = $5x10^4$; M2-Exo concentration = 50 □g mL^{-1}, M2-Exo loading frequency = three times/culture period). Untreated HT-29 cells were used as a negative control group. We conducted an RNA-seq study using NovaSeq 6000 (Illumina, USA). RNA was extracted using the RNeasy

ARTICLE IN PRESS

mini kit (Qiagen, USA), and messenger RNA was purified from total RNA using poly-T oligo-attached magnetic beads. Raw data of FASTQ format were initially processed through in-house Perl scripts to obtain clean data by removing reads containing adapter, poly-N, and low-quality reads. Differential expression analysis (DEA) of two-group comparisons (two biological replicates per condition) was performed using the DESeq2 R package (1.20.0). The resulting *p*-values were adjusted using Benjamini and Hochberg's approach for controlling the false discovery rate. Genes with an adjusted *p*-value <0.05 were assigned as differentially expressed. Genes with high significance (AKR1C3, PTGS1, SERPINE 2, HSPA6 and FAM83A) were validated by RT-qPCR. All transcriptomic analyses were performed using two biological replicates, while RT-qPCR validation was conducted with three independent biological samples.

2.9. siRNA-FAM83A transfection and optimization of gene silencing

FAM83A-siRNA (sense strain: 5′-CGAGUCACUGCCUAAUAAATT-3′ and antisense strain: 5′-UUUAUUAGGCAGUGACUCGAT-3′) and non-silencing scramble (scr)-siRNA were purchased from Qiagen (Germany). HT-29 cells ($5x10^4$) were grown in 24-well plates and after the 24-hour incubation period, cells were treated with M2-Exo (50 □g mL^{-1}) three times during 5 days of culture period for the initiation of target FAM83A metastatic gene activation. At the end of the culture period, HT-29 cells were transfected with various FAM83A- and scr-siRNA (final concentration: 10, 20, and 50 nM) through Lipofectamine™ 3000 Transfection Reagent (Thermo Fisher, USA) based on the manufacturer's directions, for the optimization of ideal silencing concentration. Scr-siRNA transfected cells and HT-29 cells without any M2-Exo induction were used as negative controls, while HT-29 cells induced with M2-Exo were used as a positive control. 48 h after siRNA transfections, RT-qPCR was performed for FAM83A to confirm the silencing of M2-Exo–mediated FAM83A gene activation in HT-29 cells. Each quantification assay was carried out using three independent biological replicates, with three

ARTICLE IN PRESS

technical replicates per biological sample. Statistical differences among multiple groups were analyzed using one-way ANOVA followed by Tukey's post hoc test.

2.10. Correlation between FAM83A silencing and M2-Exo–mediated EMT activation

To confirm the suppression of M2-Exo–mediated FAM83A-driven EMT activation in HT-29 cells, RT-qPCR was performed for metastatic (MMP-2) and EMT-associated mesenchymal (N-cadherin) markers. For this purpose, optimized HT-29 cell density ($5x10^4$), M2-Exo concentration (50 □g mL^{-1}) and loading frequency (3 times), siRNA concentration (50 nM), and transfection time (48 h) were used for the RT-qPCR experiments. Scr-siRNA transfected cells and HT-29 cells without any M2-Exo induction were used as negative controls, while HT-29 cells induced with M2-Exo were used as a positive control. Each quantification assay was carried out using three independent biological replicates, with three technical replicates per biological sample. Statistical differences among multiple groups were analyzed using one-way ANOVA followed by Tukey's post hoc test.

ARTICLE IN PRESS

3. RESULTS

3.1. Isolation and Characterization of M2-Exosomes

To confirm the polarization state and functional stability of IFN-γ/IL-10-induced RAW264.7 macrophages, RT-qPCR analyses were performed to evaluate the expression of M2-specific gene markers *CD163* and *STAT6*. LPS-induced macrophages were used as a comparison group and assessed for M1-specific markers *CD64* and *STAT1*. Gene expression analysis revealed that *CD163* and *STAT6* mRNA levels were significantly upregulated in IFN-γ/IL-10-induced macrophages, whereas *CD64* and *STAT1* (M1 phenotype) were significantly upregulated in the LPS-induced group (**Figure 1A**). These findings confirm that RAW264.7 cells can be effectively polarized into the M2

ARTICLE IN PRESS

phenotype, enabling their use in downstream analyses of pro-tumorigenic activity and the isolation of M2-Exo. The presence of M2-Exo was verified through BCA protein assay, TEM, and NTA. The total protein concentration of the purified exosomes was measured to be 6 mg/mL (**Figure S1**). TEM imaging confirmed the presence of nano-sized vesicles with characteristic cup-shaped morphology ranging from 50 to 200 nm in diameter (**Figure 1B**), which is consistent with the expected size range of exosomes. Western blot analysis further validated the exosomal identity by demonstrating positive expression of classical exosome markers CD63 and CD81 (**Figure 1C and Figure S2**). NTA measurements revealed a particle concentration of 2.2×10^{10} exosomes/mL, with most particles peaking around 130 nm in size (**Figure 1D**). Additionally, DiI fluorescence labeling confirmed successful uptake of M2-Exo by HT-29 cells, as indicated by pronounced red fluorescence localized in the perinuclear region (**Figure S3**), supporting efficient internalization of M2-Exo by the target cells. Although M2 macrophages expressed CD206 and TGF-β, these markers were not detected in untreated HT-29 cells, nor in HT-29 cells following M2-Exo exposure (**Figure S4**). This negative result likely reflects the low abundance of these exosomal proteins, which may fall below the detection threshold in total cell lysates, despite confirmed exosome internalization.

ARTICLE IN PRESS

Figure 1 is here

3.2. Proof-of-Concept: M2 macrophages–HT-29 co-culture and investigation of immune-mediated EMT process

Our central hypothesis posits that immune system cells may promote EMT dynamics, promoting a phenotype switch in cancer cells through an exosome-mediated mechanism. To investigate this, a co-culture study was initially conducted using Transwell systems (**Figure 2A**). Inverted microscope images obtained after co-culture of HT-29 cells (seeded in the lower compartment) and M2 macrophages (in the upper insert) at different cell ratios (HT-29:M2

ARTICLE IN PRESS

= 1:2, 1:1, and 2:1) are shown in **Figure 2A**. HT-29 cells co-cultured at 1:1 and 2:1 ratios displayed colony morphologies similar to those of non-co-cultured controls. However, at the 1:2 ratio, colonies appeared smaller and more dispersed, indicating potential alterations in cellular organization under high M2 macrophage density (**Figure 2B**). Notably, no negative effects on cellular viability were observed across conditions (**Figure 2C**). Given that these morphological changes might reflect altered epithelial architecture or reduced cell–cell adhesion, immunofluorescence staining for EMT markers was performed at the 1:2 ratio. In monocultured HT-29 cells, strong E-cadherin (E-Cad) expression was observed, whereas N-cadherin (N-Cad) expression was negligible (**Figure 2D**). In contrast, co-culture with M2 macrophages led to a marked decrease in E-Cad and a concomitant increase in N-Cad expression, suggesting induction of a mesenchymal phenotype in HT-29 cells. To support these observations, RT-qPCR analysis of EMT-related gene expression was performed across different cell ratios. No significant changes in *E-Cad* or *N-Cad* expression were detected at the 2:1 ratio, indicating that low M2 macrophage density had minimal effect on EMT (**Figure 2E**). However, at the 1:1 ratio, *E-Cad* expression was significantly reduced (~4-fold; $p = 9.55 \times 10^{-8}$) and *N-Cad* expression increased similarly (~4-fold) compared to the 2:1 condition. The most pronounced changes were observed at the 1:2 ratio: *E-Cad* expression was decreased by ~2.4-fold ($p = 9.99 \times 10^{-10}$), while *N-Cad* expression showed an approximately 9-fold increase ($p = 1.14 \times 10^{-7}$). Furthermore, *MMP2* and *MMP9* expression levels exhibited a positive correlation with increasing M2 macrophage density, consistent with enhanced matrix remodeling associated with EMT under the influence of M2 macrophages. (**Figure 2E**). Collectively, these results confirm that co-culture with M2 macrophages induces a mesenchymal phenotype in HT-29 cells, consistent with the activation of EMT and enhanced matrix remodeling with disruption of epithelial organization.

Figure 2 is here

ARTICLE IN PRESS

3.3. Examining the role of exosomes in immune-mediated EMT activation

To determine whether M2 macrophage-induced EMT in HT-29 cells occurs through an exosome-mediated mechanism, M2-Exo were applied to HT-29 cells under varying experimental conditions, followed by assessment of matrix metalloproteinase gene expression associated with the phenotypic transition. Initially, M2-Exo at a concentration of 100 µg/mL was administered to HT-29 cells seeded at different densities (5×10^4, 1×10^5, and 2×10^5 cells per well) and cultured for 5 days. Untreated HT-29 cells served as controls. Inverted phase-contrast microscopy revealed notable alterations in epithelial morphology across all M2-Exo–treated groups (false-colored in red), suggestive of a transition toward mesenchymal morphology (**Figure 3A, B**). This morphological shift was more prominent in cultures with lower initial HT-29 cell numbers. In contrast, no evidence of EMT was observed in control groups lacking M2-Exo treatment. Cell viability and proliferation assays confirmed that M2-Exo application did not induce cytotoxic effects across any of the tested cell densities (**Figure 3C, D**). RT-qPCR analysis of EMT-related gene expression showed that *E-Cadherin* expression was significantly downregulated ($p = 3 \times 10^{-4}$) in the high-density group (2×10^5 cells) compared to the lower-density (5×10^4) and moderate-density (1×10^5) groups. Conversely, *N-Cadherin* expression was significantly higher in the low-density group compared to moderate and high-density conditions ($p = 1.9 \times 10^{-4}$), indicating enhanced mesenchymal transition at lower cell numbers (**Figure 3E**).

Figure 3 is here

To investigate the effect of exosome dosage on M2-Exo–induced EMT in HT-29 cells, varying concentrations of M2-Exo (50, 100, and 200 µg/mL) were applied to HT-29 cells (5×10^4 cells/well) and cultured for 5 days. Across all three concentrations, HT-29 cells exhibited a clear transition from epithelial

ARTICLE IN PRESS

to mesenchymal morphology, displaying bipolar and spindle-shaped mesenchymal features (**Figure 4A**). In contrast, untreated cells maintained typical epithelial morphology characterized by colony-like expansion. To evaluate whether higher exosome concentrations had any cytotoxic or anti-proliferative effects, Calcein-AM/EthD-1 live/dead staining and XTT assays were performed. The live/dead assay showed predominant green fluorescence and negligible red signal, indicating maintained viability at all concentrations (**Figure 4B**). Similarly, the XTT assay revealed comparable proliferation kinetics among all M2-Exo–treated groups and the control, with an approximate 70% increase in proliferation from day 2 to day 5 (**Figure 4C**). RT-qPCR analysis was conducted to assess the impact of M2-Exo on EMT-related gene expression (**Figure 4D**). *E-Cadherin* expression was downregulated in all M2-Exo–treated groups compared to the untreated control, with the most significant reduction observed in the 50 µg/mL group (~2-fold decrease; $p = 7.1 \times 10^{-5}$). Conversely, *N-Cadherin* expression increased by 3.9-fold ($p = 2.5 \times 10^{-7}$) and 2.4-fold ($p = 3.1 \times 10^{-4}$) at 50 and 100 µg/mL doses, respectively. These findings were further supported by elevated expression of metastasis-associated genes. *MMP2* and *MMP9* expression levels were significantly upregulated in cells treated with 50 µg/mL of M2-Exo by 8-fold ($p = 2.9 \times 10^{-7}$) and 2-fold ($p = 3.6 \times 10^{-5}$), respectively, compared to the control group. While *MMP9* expression remained relatively constant across all M2-Exo concentrations, *MMP2* expression increased by 1.6-fold and 2-fold in the 100 and 200 µg/mL groups, respectively. Notably, lower M2-Exo concentrations (0–50 µg/mL) resulted in more modest increases in *N-Cadherin* and metastatic gene expression (**Figure S5**). To validate these gene expression findings at the protein level, HT-29 cells (5×10^4) were treated with 50 µg/mL M2-Exo for 5 days, followed by immunofluorescence staining for E-Cadherin and N-Cadherin. As expected, untreated cells exhibited strong E-Cadherin and minimal N-Cadherin expression, while M2-Exo–treated cells displayed reduced E-Cadherin and prominent N-Cadherin expression (**Figure 4E** and **Figure S6**).

ARTICLE IN PRESS

Collectively, these findings demonstrate that M2-Exo induces EMT in HT-29 cells in a dose-dependent manner, giving rise to a motile and mesenchymal phenotype.

Figure 4 is here

Finally, an optimization study of M2-Exo loading frequency was conducted for the M2-Exo–induced HT-29 cells in vitro model. This study was designed to more realistically mimic the in vivo environment where cellular signaling occurs permanently, as depicted in **Figure 5A**. To this end, a cellular proliferation assay was performed following 1-time, 2-time, and 3-time M2-Exo treatment during a 5-day culture period, revealing no significant difference between groups receiving 1-time, 2-times, or 3-times M2-Exo and the group without M2-Exo administration (**Figure 5B**). Similarly, Calcein-AM/Ethd-1 staining was conducted to investigate the potential effects of exosome loading frequency on cellular viability, showing no negative impact on cellular viability (**Figure 5C**). However, compared to the group without M2-Exo treatment, approximately a 10-fold decrease in E-Cad expression was observed in HT-29 cells treated with M2-Exo for 1-, 2-, and 3-times, while N-Cad expressions exhibited approximately 3.9 (p=1x10^{-4}), 31 (p=2.7x10^{-5}), and 34-fold (p=6x10^{-5}) increases, respectively (**Figure 5D**). Similarly, statistically significant and substantial increases were observed in MMP2 and MMP9 expressions in cells treated with M2-Exo for 1-, 2-, and 3-times compared to untreated HT-29 cells. Considering these results, it is concluded that increasing the frequency of M2-Exo loading leads to significant increases in EMT accompanied by higher expression of metalloproteases in HT-29 cells, with an optimal loading frequency of 3 times.

Figure 5 is here

3.4. Transcriptome analysis to decode the underlying mechanism of M2-Exo–induced EMT activation

ARTICLE IN PRESS

Figure 6 is here

To elucidate the molecular signatures associated with M2-Exo–mediated post-tumorigenic mechanisms, HT-29 cells were exposed to M2-Exo. Cells co-cultured with M2 macrophages served as a positive control, while untreated cells were utilized as a negative control. Our working hypothesis posited that M2-Exo internalization by cells would induce alterations in the transcriptomic landscape of HT-29 cells, potentially instigating EMT. Prior to transcriptome analysis, qPCR assays targeting EMT and matrix metalloproteinase were repeated to validate the involvement of exosome-mediated mechanisms in the samples. Subsequent qPCR analysis of M2-Exo–treated HT-29 cells unveiled a downregulation of E-Cadherin expression and an upregulation of N-Cadherin, MMP2, and MMP9 expression, in accordance with our previous findings (**Figure 6A**). Principal component analysis (PCA) of the RNA-seq data demonstrated distinct clustering of the experimental groups (**Figure 6B**). A Venn diagram highlighted 314 transcripts uniquely altered in M2-Exo–treated HT-29 cells, underscoring their contribution to group separation (**Figure 6C**). A Heat-Map diagram illustrated the distinctive transcriptomic pattern formed by these transcripts compared to others (**Figure 6D**). Volcano plots were generated to visually represent the significantly upregulated or downregulated transcripts. Notably, in HT-29 cells co-cultured with M2 macrophages, transcripts such as ERRFI1 (fold change=1.3, $p=1.74x10^{-13}$), RBMS2P1 (fold change=3.5, p=0.0001), and CKMT1B (fold change=1.52, p=0.0006) exhibited marked regulation (**Figure 6E**), whereas M2-Exo–treated HT-29 cells showed significant upregulation of genes like LINCO1559 (fold change=1.52, $p=2.87x10^{-48}$), AKR1C2 (fold change=2.2, $p=1.39x10^{-30}$), and FLNA (fold change=2.1, $p=1.12x10^{-9}$) (**Figure 6F**). Further analysis of highly expressed transcripts in M2-Exo–treated HT-29 cells compared to M2 macrophage co-cultured cells revealed prominent genes such as LINCO1559, AKR1C2, FAM83A, PTGS1, and AKR1C3 (**Figure 6G**). Pathway analysis utilizing KEGG pathways [22,23] unveiled alterations in gene expression

ARTICLE IN PRESS

levels associated with chemical carcinogenesis, cancer-related proteoglycans, central carbon metabolism in cancer, transcriptional misregulation in cancer, and other pathways in M2-Exo–treated HT-29 cells, aligning with previous findings (**Figure 6H**). Validation via RT-qPCR corroborated the RNA-seq results, particularly for the upregulation of PTGS1, AKR1C3, FAM83A, SERPINE, and HSPP6A in M2-Exo–treated HT-29 cells but not in M2 macrophage co-cultured cells (**Figure 6I**). Notably, FAM83A emerged as statistically significant for its upregulation in M2-Exo–treated HT-29 cells (fold change=3.6, $p=7.64x10^{-8}$) compared to M2 macrophage co-cultured cells, underscoring its relevance as a key exosome-driven regulator of EMT.

3.5 Silencing FAM83A for the validation of FAM83-mediated EMT activation

In this study, significant insights were obtained into the immune-mediated activation of EMT. RNA-seq analysis revealed that exosomes derived from M2 macrophages upregulate *FAM83A* expression in HT-29 cells. To investigate the role of *FAM83A* in EMT, a specific siRNA targeting *FAM83A* was designed and optimized, followed by gene expression analysis. Under basal conditions, HT-29 cells exhibited low *FAM83A* expression. However, upon stimulation with M2-Exo, *FAM83A* levels increased approximately 2-fold (p = 0.0027). Treatment with siRNA-FAM83A at 10, 20, and 50 nM resulted in a significant and dose-dependent downregulation of *FAM83A* (**Figure 7A**), whereas no significant changes were observed in cells treated with equivalent doses of scramble siRNA (scr). These findings confirm the effective silencing capability of the designed siRNA. To further elucidate the role of *FAM83A* in EMT and early tumor-progressive phenotypes, *N-Cadherin* and *MMP2* expression levels were analyzed by RT-qPCR in HT-29 cells treated with M2-Exo, siRNA-FAM83A, and scr (**Figure 7B,C**). While M2-Exo treatment led to upregulation of both *N-Cad* and *MMP2*, a dose-dependent suppression of these genes was observed following siRNA-FAM83A transfection. In contrast,

ARTICLE IN PRESS

no such reduction was observed in the scramble-treated groups, indicating that *FAM83A* upregulation plays a central role in M2-Exo–induced EMT. To validate these findings at the protein level, Western blot analysis for E-Cadherin and N-Cadherin was performed (**Figure 7D and Figure S7- S8**). As expected, HT-29 cells under basal conditions expressed both markers. M2-Exo treatment resulted in a marked increase in N-Cadherin levels, supporting its EMT-inducing potential. Co-treatment with an Akt inhibitor, given Akt's known association with EMT and N-Cadherin upregulation, led to a moderate reduction in N-Cadherin expression. Notably, cells treated with both M2-Exo and siRNA-FAM83A exhibited a more pronounced decrease in N-Cadherin levels, further validating the central role of *FAM83A*. Moreover, combined treatment with M2-Exo, siRNA-FAM83A, and the Akt inhibitor resulted in a substantial suppression of N-Cadherin expression, emphasizing the synergistic inhibitory effect on EMT activation.

To evaluate the broader applicability of our hypothesis and model beyond colorectal cancer, *FAM83A* expression levels were assessed by RT-qPCR in other cancer cell lines, including breast cancer (MCF-7), melanoma (451LU), and glioblastoma (T98G) cells. The results showed high *FAM83A* expression in MCF-7 cells, while low expression was detected in both melanoma and glioblastoma lines (**Figure S9**). These preliminary findings suggest that the M2-Exo–*FAM83A*–EMT axis may be more relevant in specific tumor types, warranting further investigation into the role of *FAM83A* in EMT activation across various cancers.

Figure 7 is here

4. Discussion

The results of this study provide compelling evidence of the involvement of M2 macrophages and M2-Exosomes in activating EMT in HT-29 cells. Co-culture with M2 macrophages decreased epithelial phenotype and induced a

ARTICLE IN PRESS

mesenchymal phenotype in HT-29 cells, evidenced by the downregulation of E-Cadherin and the upregulation of N-Cadherin expression levels (**Figure 2D,E**), similar to literature studies.[24,25] Further investigations revealed that M2-Exosome application led to the initiation of mesenchymal morphology in HT-29 cells (**Figure 3A**), with a transition from epithelial to mesenchymal cell morphology observed across different cell ratios and exosome concentrations (**Figure 3E, 4D**). Notably, gene expression analyses confirmed the downregulation of E-Cadherin and upregulation of N-Cadherin in M2-Exo–treated HT-29 cells, accompanied by increased expression of metastatic markers MMP2 and MMP9 (**Figure 4D**). Immunofluorescence staining validated these findings (**Figure 4E**), emphasizing the pivotal role of M2 macrophage–derived exosomes in EMT activation. These findings offer important insights into how M2 macrophages drive EMT activation and establish pre-metastatic transcriptional conditioning within the tumor microenvironment, highlighting their potential influence on immune-mediated cancer progression. When reviewing the studies reported in the literature, it is evident that investigations into the post-tumorigenic effects of M2 macrophage exosomes are being conducted. These studies provide insights into EMT-like alterations and pro-migratory/invasive behaviors at a molecular level. For instance, Lu et al. reported that M2 macrophage exosomes promote EMT characteristics in hepatocellular carcinoma cells through miR-23a-3p regulation.[26] In a different study focusing on miRNA-mediated mechanisms, M2 macrophage exosomes delivering miR-21-5p and miR-155-5p were shown to downregulate BRG1 in colon cancer cells. This BRG1 suppression was accompanied by enhanced migration and invasion, aligning with a shift toward a more invasive, EMT-associated cellular phenotype.[27] Furthermore, a separate study highlighted that M2 macrophage exosomes facilitate migration and promote metastasis in non-small-cell lung cancer cells through the mechanism involving integrin aVb3.[28] Zheng et al. reported that M2 macrophage exosomes enhance the metastatic migratory abilities of gastric cancer cells by influencing the

ARTICLE IN PRESS

function of Apolipoprotein E.[29] In this study, we investigated the EMT phase of the metastatic cascade by defining the EMT-like transcriptional alterations induced by M2 macrophage–derived exosomes and elucidating how M2-Exo–driven proto-oncogene activation promotes EMT-associated cancer progression.

The comprehensive analysis conducted in this study elucidated the molecular signatures associated with M2-Exosome-mediated post-tumorigenic mechanisms in HT-29 cells. The observed alterations in the transcriptomic landscape, including the differential gene expression profiles between M2-Exo–treated HT-29 cells and M2 macrophage co-cultured cells (**Figure 6B-D**), particularly the significant upregulation of genes like FAM83A (**Figure 6G**), highlight the potential involvement of M2-Exosome-mediated mechanisms in EMT-mediated cancer progression. These findings highlight the need for deeper investigation into the roles of FAM83A and other identified genes in the EMT-initiated cellular transitions that contribute to the metastatic cascade driven by M2-Exo exposure.

Studies have suggested a potential relationship between the FAM83A gene and EMT-related cancer progression. FAM83A has been reported to be involved in promoting cancer metastasis by enhancing cell migration, invasion, and metastatic potential.[30,31] High FAM83A expression levels have been associated with EMT markers, indicating a possible role in elevated metastatic behavior.[32] Moreover, FAM83A overexpression has been linked to drug resistance in cancer treatments, potentially contributing to metastatic progression.[33] Elevated FAM83A levels have been associated with poor prognosis and increased metastasis in various cancer types, suggesting its potential as a prognostic marker for metastatic disease. The relation between the FAM83A gene and colorectal cancer has been newly discovered.[34] FAM83A is overexpressed in colorectal cancer cells and clinical samples, indicating its involvement in the disease's development and

ARTICLE IN PRESS

progression. High FAM83A levels correlate with advanced tumor stages, poorer prognosis, and increased metastasis in colorectal cancer patients, suggesting its potential as a prognostic marker. The overexpression and phosphorylation of FAM83A activates key signaling pathways such as Wnt/β-catenin,[35] EGFR,[36] and PI3K, known to drive cancer progression. Hence, FAM83A has been proposed as a viable therapeutic target, with its inhibition potentially hindering tumor growth, metastasis, and drug resistance in colorectal cancer. Although previous studies implicate FAM83A in metastatic progression, determining whether its regulation under immune exosome–induced EMT activation serves as a proto-oncogenic driver that primes cells for metastatic competence remains crucial.

In this study, we confirmed the involvement of FAM83A in EMT, suggesting its potential contribution to subsequent progression in colorectal cancer. Targeting FAM83A using siRNA resulted in a significant reduction in its expression levels, highlighting the efficacy of the designed siRNA (**Figure 7A**). Subsequent examination of N-Cadherin and MMP2 gene expressions demonstrated a notable increase in M2-Exo–treated HT-29 cells, whereas siRNA-mediated FAM83A silencing led to a dose-dependent decrease in these markers (**Figure 7B-C**). These findings indicate that M2-Exo–mediated upregulation of FAM83A functionally promotes transcriptional programs associated with EMT in colorectal cancer cells, a process recognized as a key initiating step in the metastatic cascade. Evaluation of FAM83A expression across additional cancer cell lines revealed variable patterns among tumor types, highlighting its potential role in modulating EMT dynamics in diverse cancer contexts **(Figure 7D).** Further studies are warranted to elucidate the precise mechanisms by which FAM83A orchestrates EMT-related changes that enable cancer cells to acquire invasive and migratory phenotypes.

5. Conclusion

ARTICLE IN PRESS

The findings from this study shed light on the crucial role of M2-Exo in enhancing FAM83A expression to activate EMT and facilitate early metastatic progression. This finding underscores that exosomes derived from M2 macrophages act as potent mediators of EMT induction, exerting a stronger effect than the parental M2 cells themselves. The exosomal cargo not only triggers EMT programs but also upregulates the proto-oncogene FAM83A, highlighting that exosome-mediated signaling drives both phenotypic plasticity and oncogenic transcriptional changes in recipient tumor cells. Moreover, our findings support a functional involvement of exosomes in immune–cancer crosstalk. Specifically, the upregulation of FAM83A following exposure to M2 macrophage–derived exosomes, together with its association with EMT-related transcriptional changes, suggests a potential link between exosome-mediated signaling and EMT modulation in cancer cells. These observations provide a rationale for future studies to further investigate the molecular mechanisms underlying exosome-associated tumor cell plasticity. Addressing these strategies is pivotal for devising effective therapeutic interventions targeting cancer metastasis. Moving forward, further investigations are warranted to scrutinize the protein-level implications of the results, delve into detailed pathway analyses, assess potential side effects of FAM83A gene silencing, evaluate the consequences of inhibiting M2-exosome secretion, and conduct in vivo studies. These gaps in the current study emphasize the necessity for advanced research to fill these voids comprehensively. The insights gained from this study pave the way for future investigations aimed at elucidating the intricate dynamics of EMT-related processes and devising targeted interventions.

ARTICLE IN PRESS

References

[1] A. van Weverwijk, K.E. de Visser, Mechanisms driving the immunoregulatory function of cancer cells, Nature Reviews Cancer 2023 23:4 23 (2023) 193–215. https://doi.org/10.1038/s41568-022-00544-4.

ARTICLE IN PRESS

[2] S.H. Chan, W.H. Kuo, L.H. Wang, SCEL regulates switches between pro-survival and apoptosis of the TNF-α/TNFR1/NF-κB/c-FLIP axis to control lung colonization of triple negative breast cancer, J Biomed Sci 30 (2023) 1–22. https://doi.org/10.1186/S12929-023-00986-4/FIGURES/9.

[3] A.E. Ryan, A. Colleran, A. O'Gorman, L. O'Flynn, J. Pindjacova, P. Lohan, G. O'Malley, M. Nosov, C. Mureau, L.J. Egan, Targeting colon cancer cell NF-κB promotes an anti-tumour M1-like macrophage phenotype and inhibits peritoneal metastasis, Oncogene 2015 34:12 34 (2014) 1563–1574. https://doi.org/10.1038/onc.2014.86.

[4] A. Mantovani, P. Allavena, F. Marchesi, C. Garlanda, Macrophages as tools and targets in cancer therapy, Nature Reviews Drug Discovery 2022 21:11 21 (2022) 799–820. https://doi.org/10.1038/s41573-022-00520-5.

[5] J. Zhou, N. Lyu, Q. Wang, M. Yang, E.T. Kimchi, K. Cheng, T. Joshi, A.R. Tukuli, K.F. Staveley-O'Carroll, G. Li, A novel role of TGFBI in macrophage polarization and macrophage-induced pancreatic cancer growth and therapeutic resistance, Cancer Lett 578 (2023) 216457. https://doi.org/10.1016/J.CANLET.2023.216457.

[6] X.L. Zhang, L.P. Hu, Q. Yang, W.T. Qin, X. Wang, C.J. Xu, G.A. Tian, X.M. Yang, L.L. Yao, L. Zhu, H.Z. Nie, Q. Li, Q. Xu, Z.G. Zhang, Y.L. Zhang, J. Li, Y.H. Wang, S.H. Jiang, CTHRC1 promotes liver metastasis by reshaping infiltrated macrophages through physical interactions with TGF-β receptors in colorectal cancer, Oncogene 2021 40:23 40 (2021) 3959–3973. https://doi.org/10.1038/s41388-021-01827-0.

[7] S.C. Lin, Y.C. Liao, P.M. Chen, Y.Y. Yang, Y.H. Wang, S.L. Tung, C.M. Chuang, Y.W. Sung, T.H. Jang, S.E. Chuang, L.H. Wang, Periostin promotes ovarian cancer metastasis by enhancing M2 macrophages and cancer-associated fibroblasts via integrin-mediated NF-κB and TGF-β2 signaling, J Biomed Sci 29 (2022) 1–17. https://doi.org/10.1186/S12929-022-00888-X/FIGURES/7.

[8] Q. Liu, C. Yang, S. Wang, D. Shi, C. Wei, J. Song, X. Lin, R. Dou, J. Bai, Z. Xiang, S. Huang, K. Liu, B. Xiong, Wnt5a-induced M2 polarization of tumor-associated macrophages via IL-10 promotes colorectal cancer progression, Cell Communication and Signaling 18 (2020) 1–19. https://doi.org/10.1186/S12964-020-00557-2/FIGURES/7.

[9] S. Chen, M. Wang, T. Lu, Y. Liu, W. Hong, X. He, Y. Cheng, J. Liu, Y. Wei, X. Wei, JMJD6 in tumor-associated macrophage regulates macrophage polarization and cancer progression via STAT3/IL-10 axis, Oncogene 2023 42:37 42 (2023) 2737–2750. https://doi.org/10.1038/s41388-023-02781-9.

[10] H. Yang, Q. Zhang, M. Xu, L. Wang, X. Chen, Y. Feng, Y. Li, X. Zhang, W. Cui, X. Jia, CCL2-CCR2 axis recruits tumor associated macrophages to induce immune evasion through PD-1 signaling in esophageal carcinogenesis, Mol Cancer 19 (2020) 1–14. https://doi.org/10.1186/S12943-020-01165-X/FIGURES/7.

ARTICLE IN PRESS

[11] V. Gómez, T.R. Eykyn, R. Mustapha, F. Flores-Borja, V. Male, P.R. Barber, A. Patsialou, R. Green, F. Panagaki, C.W. Li, G.O. Fruhwirth, S. Ros, K.M. Brindle, T. Ng, Breast cancer-associated macrophages promote tumorigenesis by suppressing succinate dehydrogenase in tumor cells, Sci Signal 13 (2020) 4585. https://doi.org/10.1126/SCISIGNAL.AAX4585/SUPPL_FILE/AAX4585_SM.PDF.

[12] I. Hwang, J.W. Kim, K. Ylaya, E.J. Chung, H. Kitano, C. Perry, J. Hanaoka, J. Fukuoka, J.Y. Chung, S.M. Hewitt, Tumor-associated macrophage, angiogenesis and lymphangiogenesis markers predict prognosis of non-small cell lung cancer patients, J Transl Med 18 (2020) 1–15. https://doi.org/10.1186/S12967-020-02618-Z/FIGURES/5.

[13] M.A. Kumar, S.K. Baba, H.Q. Sadida, S. Al Marzooqi, J. Jerobin, F.H. Altemani, N. Algehainy, M.A. Alanazi, A.B. Abou-Samra, R. Kumar, A.S. Al-Shabeeb Akil, M.A. Macha, R. Mir, A.A. Bhat, Extracellular vesicles as tools and targets in therapy for diseases, Signal Transduction and Targeted Therapy 2024 9:1 9 (2024) 1–41. https://doi.org/10.1038/s41392-024-01735-1.

[14] E. Yang, X. Wang, Z. Gong, M. Yu, H. Wu, D. Zhang, Exosome-mediated metabolic reprogramming: the emerging role in tumor microenvironment remodeling and its influence on cancer progression, Signal Transduction and Targeted Therapy 2020 5:1 5 (2020) 1–13. https://doi.org/10.1038/s41392-020-00359-5.

[15] Y. Guo, X. Ji, J. Liu, D. Fan, Q. Zhou, C. Chen, W. Wang, G. Wang, H. Wang, W. Yuan, Z. Ji, Z. Sun, Effects of exosomes on pre-metastatic niche formation in tumors, Molecular Cancer 2019 18:1 18 (2019) 1–11. https://doi.org/10.1186/S12943-019-0995-1.

[16] K. Stefańska, M. Józkowiak, A. Angelova Volponi, J.A. Shibli, A. Golkar-Narenji, P. Antosik, D. Bukowska, H. Piotrowska-Kempisty, P. Mozdziak, P. Dzięgiel, M. Podhorska-Okołów, M. Zabel, M. Dyszkiewicz-Konwińska, B. Kempisty, The Role of Exosomes in Human Carcinogenesis and Cancer Therapy—Recent Findings from Molecular and Clinical Research, Cells 2023, Vol. 12, Page 356 12 (2023) 356. https://doi.org/10.3390/CELLS12030356.

[17] R. Raguraman, D. Bhavsar, D. Kim, X. Ren, V. Sikavitsas, A. Munshi, R. Ramesh, Tumor-targeted exosomes for delivery of anticancer drugs, Cancer Lett 558 (2023) 216093. https://doi.org/10.1016/J.CANLET.2023.216093.

[18] M. Zhou, X. He, C. Mei, C. Ou, Exosome derived from tumor-associated macrophages: biogenesis, functions, and therapeutic implications in human cancers, Biomarker Research 2023 11:1 11 (2023) 1–17. https://doi.org/10.1186/S40364-023-00538-W.

[19] M. Sungu, M. Isik, Ü. Güler, C.C. Eylem, H. Eskizengin, E. Nemutlu, B. Salih, B. Derkus, Manipulating macrophage polarization with nanoparticles to control metastatic behavior in heterotypic breast

ARTICLE IN PRESS

cancer micro-tissues via exosome signaling, Nanoscale 16 (2023) 394–410. https://doi.org/10.1039/D3NR04980A.
[20] B. Derkus, M. Isik, C.C. Eylem, I. Ergin, C.B. Camci, S. Bilgin, C. Elbuken, Y.E. Arslan, M. Akkulak, O. Adali, F. Kiran, B.O. Okesola, E. Nemutlu, E. Emregul, Xenogenic Neural Stem Cell-Derived Extracellular Nanovesicles Modulate Human Mesenchymal Stem Cell Fate and Reconstruct Metabolomic Structure, Adv Biol 6 (2022) 2101317. https://doi.org/10.1002/ADBI.202101317.
[21] C.C. Eylem, M. Yilmaz, B. Derkus, E. Nemutlu, C.B. Camci, E. Yilmaz, M.A. Turkoglu, B. Aytac, N. Ozyurt, E. Emregul, Untargeted multi-omic analysis of colorectal cancer-specific exosomes reveals joint pathways of colorectal cancer in both clinical samples and cell culture, Cancer Lett 469 (2020) 186–194. https://doi.org/10.1016/J.CANLET.2019.10.038.
[22] M. Kanehisa, M. Furumichi, Y. Sato, Y. Matsuura, and M. Ishiguro-Watanabe, KEGG: biological systems database as a model of the real world. Nucleic Acids Res. 53 (2025) D672-D677.
[23] M. Kanehisa and S. Goto. KEGG: Kyoto Encyclopedia of Genes and Genomes. Nucleic Acids Res. 28 (2000) 27-30.
[24] Z. Guo, J. Song, J. Hao, H. Zhao, X. Du, E. Li, Y. Kuang, F. Yang, W. Wang, J. Deng, Q. Wang, M2 macrophages promote NSCLC metastasis by upregulating CRYAB, Cell Death Dis 10 (2019). https://doi.org/10.1038/S41419-019-1618-X.
[25] M. Yang, B. Ma, H. Shao, A.M. Clark, A. Wells, Macrophage phenotypic subtypes diametrically regulate epithelial-mesenchymal plasticity in breast cancer cells, BMC Cancer 16 (2016) 1–13. https://doi.org/10.1186/S12885-016-2411-1/FIGURES/4.
[26] Y. Lu, G. Han, Y. Zhang, L. Zhang, Z. Li, Q. Wang, Z. Chen, X. Wang, J. Wu, M2 macrophage-secreted exosomes promote metastasis and increase vascular permeability in hepatocellular carcinoma, Cell Commun Signal 21 (2023). https://doi.org/10.1186/S12964-022-00872-W.
[27] J. Lan, L. Sun, F. Xu, L. Liu, F. Hu, D. Song, Z. Hou, W. Wu, X. Luo, J. Wang, X. Yuan, J. Hu, G. Wang, M2 macrophage-derived exosomes promote cell migration and invasion in colon cancer, Cancer Res 79 (2019) 146–158. https://doi.org/10.1158/0008-5472.CAN-18-0014/653225/AM/M2-MACROPHAGE-DERIVED-EXOSOMES-PROMOTE-CELL.
[28] L. Huang, F. Wang, X. Wang, C. Su, S. Wu, C. Yang, M. Luo, J. Zhang, L. Fu, M2-like macrophage-derived exosomes facilitate metastasis in non-small-cell lung cancer by delivering integrin αVβ3, MedComm (Beijing) 4 (2022) e191. https://doi.org/10.1002/MCO2.191.
[29] P. Zheng, Q. Luo, W. Wang, J. Li, T. Wang, P. Wang, L. Chen, P. Zhang, H. Chen, Y. Liu, P. Dong, G. Xie, Y. Ma, L. Jiang, X. Yuan, L. Shen, Tumor-associated macrophages-derived exosomes promote the migration of gastric cancer cells by transfer of functional Apolipoprotein E, Cell

ARTICLE IN PRESS

Death & Disease 2018 9:4 9 (2018) 1–14. https://doi.org/10.1038/s41419-018-0465-5.
[30] Y.W. Zheng, Z.H. Li, L. Lei, C.C. Liu, Z. Wang, L.R. Fei, M.Q. Yang, W.J. Huang, H.T. Xu, FAM83A Promotes Lung Cancer Progression by Regulating the Wnt and Hippo Signaling Pathways and Indicates Poor Prognosis, Front Oncol 10 (2020) 180. https://doi.org/10.3389/FONC.2020.00180/FULL.
[31] C. Zhao, X. Li, R. Zhang, H. Lyu, S. Xiao, D. Guo, D.W. Ali, M. Michalak, X.Z. Chen, C. Zhou, J. Tang, Sense and anti-sense: Role of FAM83A and FAM83A-AS1 in Wnt, EGFR, PI3K, EMT pathways and tumor progression, Biomedicine & Pharmacotherapy 173 (2024) 116372. https://doi.org/10.1016/J.BIOPHA.2024.116372.
[32] B. Zhou, X. Zhou, C. Zhan, M. Jin, S. Yan, FAM83A promotes the progression and metastasis of human pancreatic neuroendocrine tumors by inducing the epithelial-mesenchymal transition via the PI3K/AKT and ERK pathways, J Endocrinol Invest 46 (2023) 1115–1130. https://doi.org/10.1007/S40618-022-01959-4.
[33] S.Y. Lee, R. Meier, S. Furuta, M.E. Lenburg, P.A. Kenny, R. Xu, M.J. Bissell, FAM83A confers EGFR-TKI resistance in breast cancer cells and in mice, J Clin Invest 122 (2012) 3211–3220. https://doi.org/10.1172/JCI60498.
[34] Z. Liu, Y. Zhang, Q. Dang, K. Wu, D. Jiao, Z. Li, Z. Sun, X. Han, Genomic Alteration Characterization in Colorectal Cancer Identifies a Prognostic and Metastasis Biomarker: FAM83A|IDO1, Front Oncol 11 (2021). https://doi.org/10.3389/FONC.2021.632430/FULL.
[35] C. Zhou, X. Zhu, N. Liu, X. Dong, X. Zhang, H. Huang, Y. Tang, S. Liu, M. Hu, M. Wang, X. Deng, S. Li, R. Zhang, Y. Huang, H. Lyu, S. Xiao, S. Luo, D.W. Ali, M. Michalak, X.Z. Chen, Z. Wang, J. Tang, B-lymphoid tyrosine kinase-mediated FAM83A phosphorylation elevates pancreatic tumorigenesis through interacting with β-catenin, Signal Transduction and Targeted Therapy 2022 8:1 8 (2023) 1–18. https://doi.org/10.1038/s41392-022-01268-5.
[36] R. Cipriano, K.L.S. Miskimen, B.L. Bryson, C.R. Foy, C.A. Bartel, M.W. Jackson, Conserved Oncogenic Behavior of the FAM83 Family Regulates MAPK Signaling in Human Cancer, Mol Cancer Res 12 (2014) 1156. https://doi.org/10.1158/1541-7786.MCR-13-0289.

Funding Declaration

This work was financially supported by the Scientific and Technological Research Council of Turkey (TUBITAK, Grant No: 123S856).

Acknowledgements

ARTICLE IN PRESS

Burak Derkus thanks the Turkish Academy of Science (TUBA) and the Science Academy (Istanbul) for their support. We thank the Dr. Fatih Inci and Nedim Haciosmanoglu (Bilkent University, Turkey) for their kind help in NTA analysis. This paper was prepared using a part of data from Melis Isik's PhD thesis.

Author contributions

MI contributed to conceptualization, investigation, methodology and writing the original draft. MA contributed to investigation. BD contributed to methodology, resources, supervision, and writing the original draft.

Data availability statement

The transcriptomic mRNA-seq datasets generated and/or analyzed during the current study are available in the Genome Sequence Archive (GSA) under accession number HDAC008190.

Competing Interests Statement

The authors declare no conflict of interest.

ARTICLE IN PRESS

Figure Legends

Figure 1. (A) Gene expression analysis for M1-markers (STAT-1 and CD64) and M2-markers (STAT-6 and CD163) to confirm the polarization of Raw267.4 cells into M1- and M2-phenotypes. *p<0.05, **p<0.01, ***p<0.0001, NS=non-significant. (B) TEM images showing the conventional lipid-bilayer structure of M2-Exo with the size around 150 nm. (C) WB analysis for CD63 and CD81, two surface markers for exosomes. (D) Concentration-particle size spectrum (multiply with 10^{10}) and scatter graph showing the size distribution and particle concentration at median size.

Figure 2. (A) The hypothesis: Co-culture with M2 macrophages or inducing with M2-Exo induces EMT in HT-29 cells. (B) Invert phase-contrast images of HT-29 cells before and after co-culture with M2 macrophages. (C) Cell viability assay images showing the biocompatibility of co-culture conditions at 1:2, 1:1, and 2:1 cell ratio of HT-29 to M2 macrophages. (D) Immunofluorescent microscopy images obtained for E-Cad (green) and N-Cad (red), two EMT markers, obtained with HT-29 cells before and after co-culture with M2 macrophages. (E) Gene expression analyses for EMT (E-Cad

ARTICLE IN PRESS

and N-Cad) and metastasis (MMP2 and MMP9) markers at varying HT-29:M2 macrophage cell number ratio (1:2, 1:1, 2:1). All conditions for gene expression analysis were performed in triplicate using independent Transwell setups. All schematic illustrations were created by the authors using BioRender.

Figure 3. (A) Invert phase-contrast images showing the mesenchymal transiting cells upon M2-Exo induction to HT-29 cells with varying initial cell number (50K, 100K, and 200K). (B) An illustration depicting the observations in microscopical assessments. (C) Cell proliferation test showing the proliferative ability of HT-29 cells against M2-Exo induction. (D) Cell viability assay testing the biocompatibility of M2-Exo induction. (E) EMT (E-Cad and N-Cad) gene expressions in HT-29 cells treated with M2-Exo. For cell proliferation, each red dot represents a single biological replicate. All RT-qPCR experiments were performed across three independent biological replicates. All schematic illustrations were created by the authors using BioRender.

Figure 4. (A) Invert phase-contrast images showing the mesenchymal transiting cells upon M2-Exo induction with varying M2-Exo concentration (50, 100, and 200 $\mu g.mL^{-1}$). (B) Cell viability assay testing the biocompatibility of low, mid, and high doses of M2-Exo. (C) Cell proliferation test showing the proliferative ability of HT-29 cells against varying doses of M2-Exo. (D) EMT (E-Cad and N-Cad) and metastatic (MMP-2 and MMP-9) gene expressions in HT-29 cells treated with varying doses of M2-Exo. (E) Immunofluorescent images were obtained with E-Cad and N-Cad before and after M2-Exo treatment of HT-29 cells. For cell proliferation, each red dot represents a single biological replicate. All RT-qPCR experiments were performed in triplicate across three independent biological replicates.

ARTICLE IN PRESS

Figure 5. Effect of exosome loading frequency on EMT. (A) The rationality of loading frequency optimization. (B) Cell proliferation ability of HT-29 cells in response to different M2-Exo loading frequency. (C) Cell viability test for HT-29 cells treated with M2-Exo with different loading frequency. (D) Assessment of EMT in HT-29 cells after M2-Exo exposure for 1-, 2-, and 3 times. For cell proliferation, each red dot represents a single biological replicate. All RT-qPCR experiments were performed in triplicate across three independent biological replicates. All schematic illustrations were created by the authors using BioRender.

Figure 6. Transcriptomic analysis to elucidate the mechanism of M2-Exo–initiated EMT. (A) Verification of M2-Exo mediated upregulation of EMT in HT-29 cells preceding transcriptomic analysis. (B) PCA plot of RNA-seq data illustrating transcriptomic distinctions in HT-29 cells co-cultured with M2 macrophages and stimulated with M2-Exo, with HT-29 cells alone as the negative control. (C) A Venn diagram illustrating common and discriminated

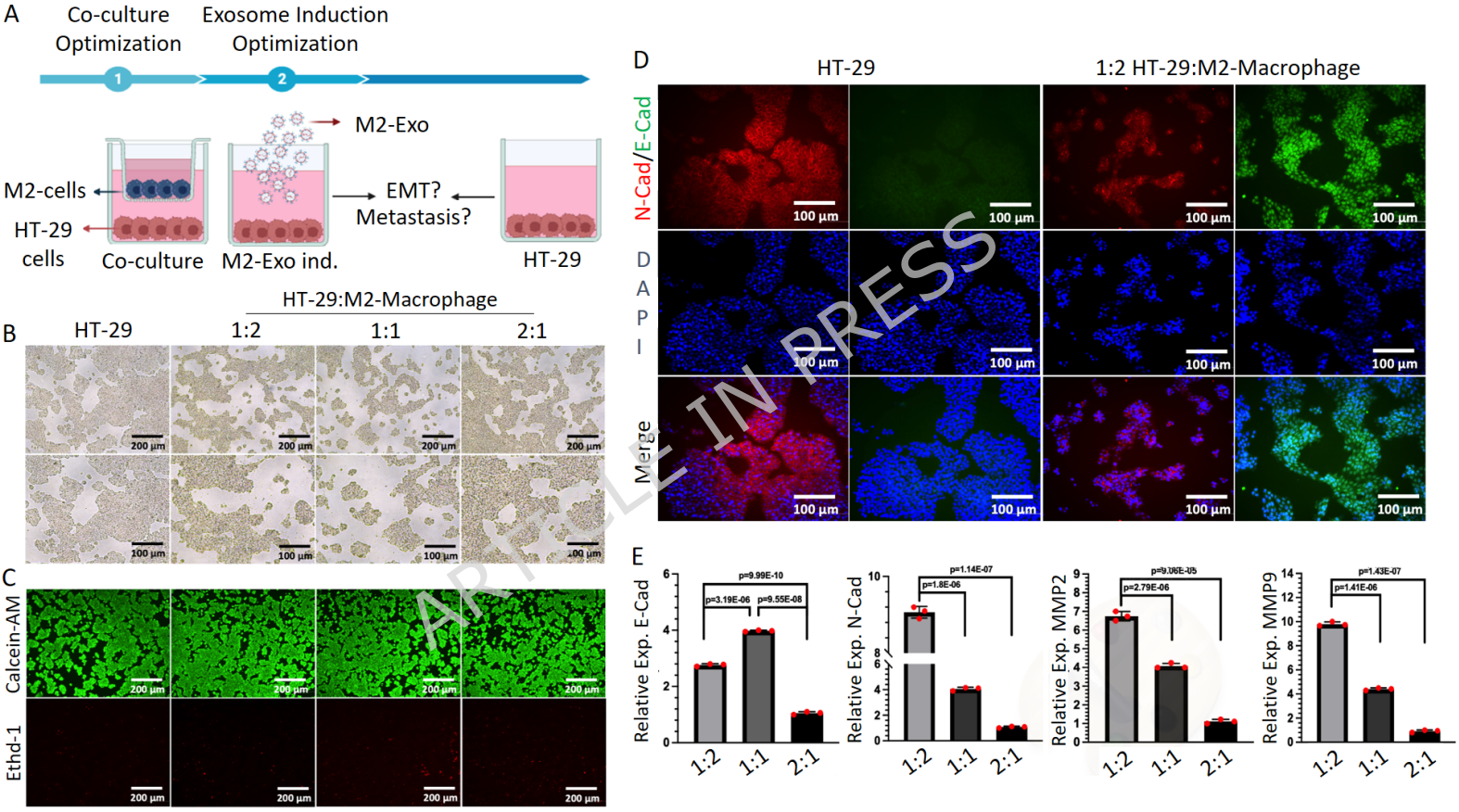
ARTICLE IN PRESS

transcript alterations across groups. (D) Hierarchical clustering analysis of transcriptomic alterations reveals distinct patterns in HT-29 cells stimulated with M2-Exo compared to both co-culture and HT-29-only groups. Volcano scatter plots illustrating differential up/down-regulation of transcripts among groups: (E) co-cultured vs HT-29 cells alone, (F) M2-Exo–stimulated HT-29 cells vs HT-29 cells alone, and (G) HT-29 cells co-cultured with M2 macrophages and stimulated with M2-Exo. (H) KEGG pathway [22,23] analysis identified gene expression changes in M2-Exo–treated HT-29 cells, consistent with cancer-related pathways. (I) Identification of EMT-related upregulated transcripts in M2-Exo stimulated HT-29 cells through transcriptome analysis, followed by RT-qPCR validation demonstrating specific upregulation mediated by M2-Exo, distinct from co-culture and HT-29-only groups. All transcriptomic analyses were performed using two biological replicates, while RT-qPCR experiments were conducted in the biological replicates.

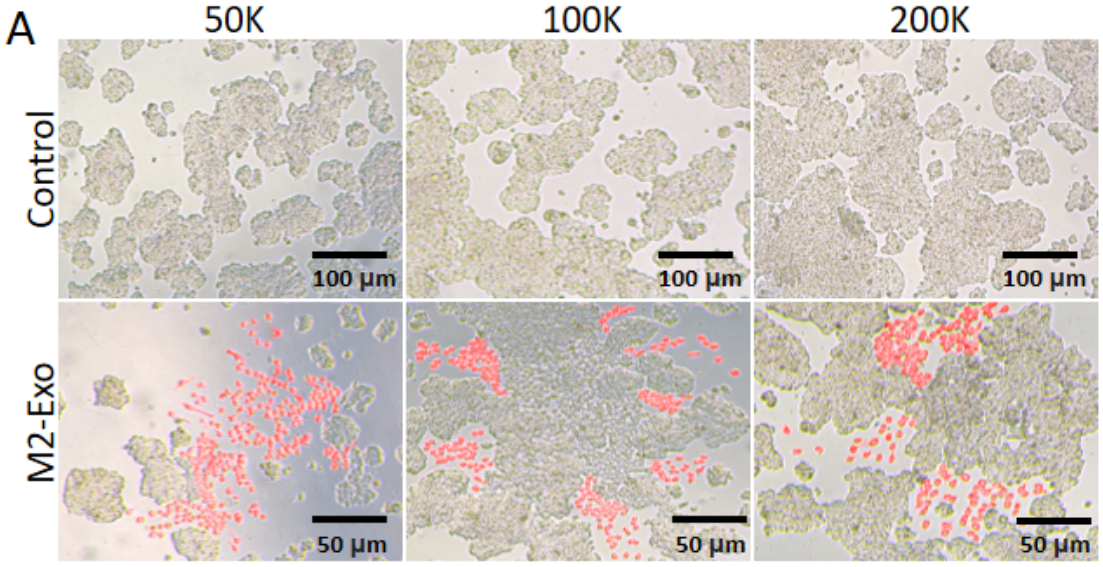
Figure 7. Validation of M2-Exo stimulated FAM83A-mediated EMT activation through FAM83A silencing and examining by RT-qPCR analysis. (A) Silencing of FAM83A in M2-Exo–induced HT-29 cells using varying concentrations of FAM83A-siRNA (sir10, 20, 50 nM) and corresponding scramble-siRNA controls (scr10, 20, 50 nM). HT-29 cells alone and HT-29 cells stimulated with M2-Exo served as negative and positive controls, respectively. Silencing FAM83A attenuates M2-Exo–mediated EMT, as demonstrated by reduced expression of the (B) mesenchymal marker N-Cadherin and (C) the metastasis marker MMP-2, in M2-Exo stimulated HT-29 cells, respectively. (D) FAM83A expression was assessed in breast cancer (MCF-7), melanoma (451LU), and glioblastoma (T98G) cells without M2-Exosome stimulation (NS = $p > 0.05$, *$p < 0.05$, **$p < 0.01$, ***$p < 0.001$). Western Blot images obtained with N-cadherin and E-cadherin to assess the response of HT-29 cells against M2-Exo, M2-Exo–Akt inhibitor co-load, M2-Exo–siRNA co-load, and M2-Exo–Akt inhibitor-siRNA co-load. RT-qPCR experiments were conducted in triplicate across three biological replicates. Western blot analysis was performed in duplicate using protein samples pooled from three independent biological replicates.

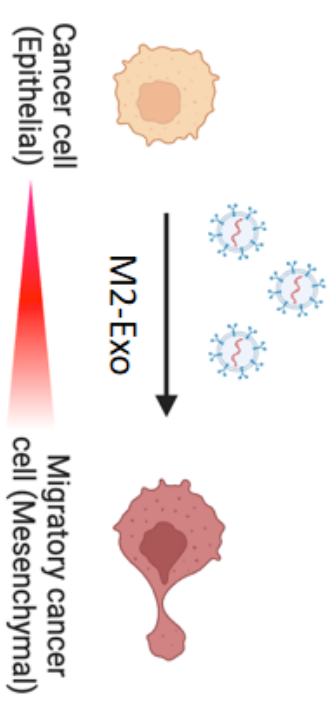
ARTICLE IN PRESS

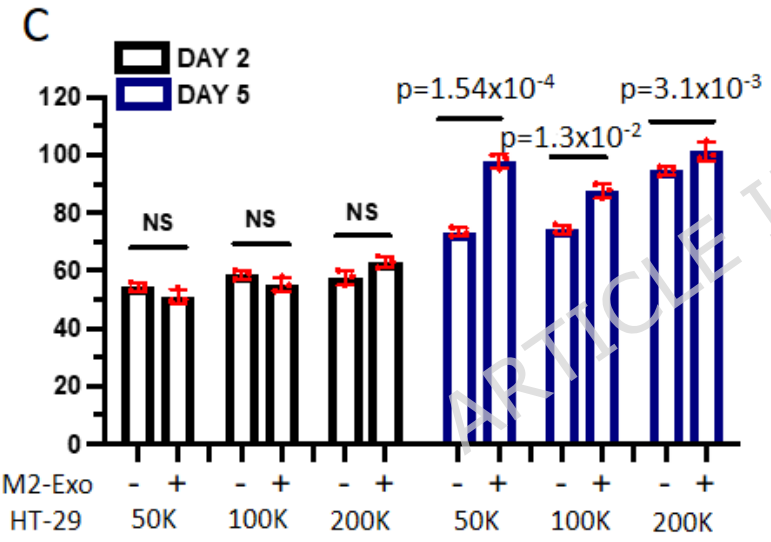
ARTICLE IN PRESS

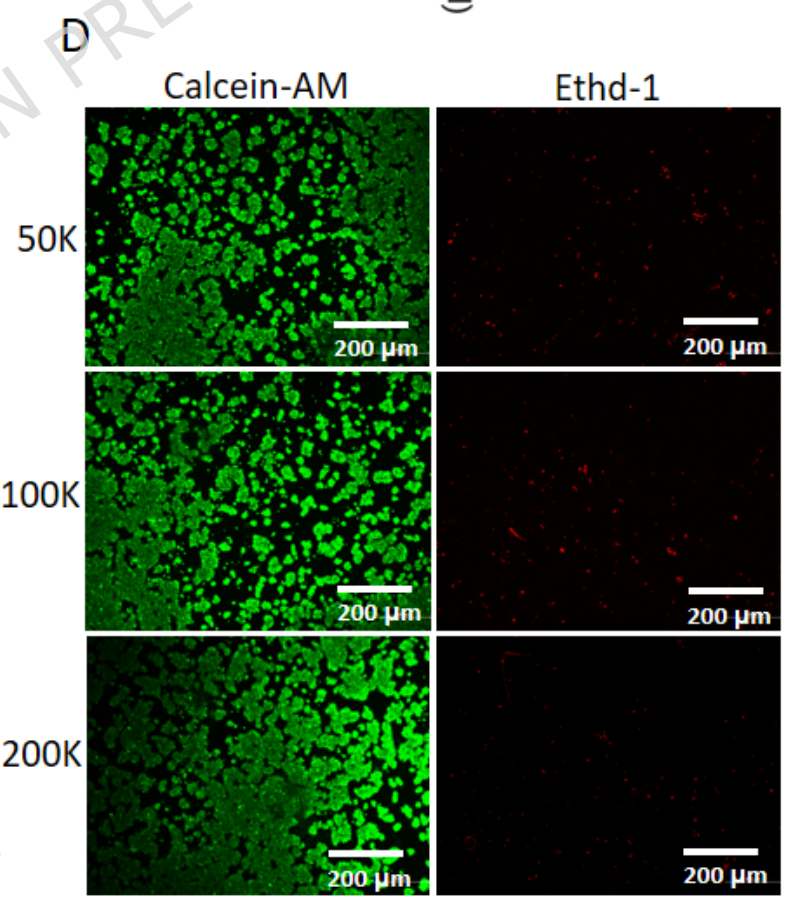


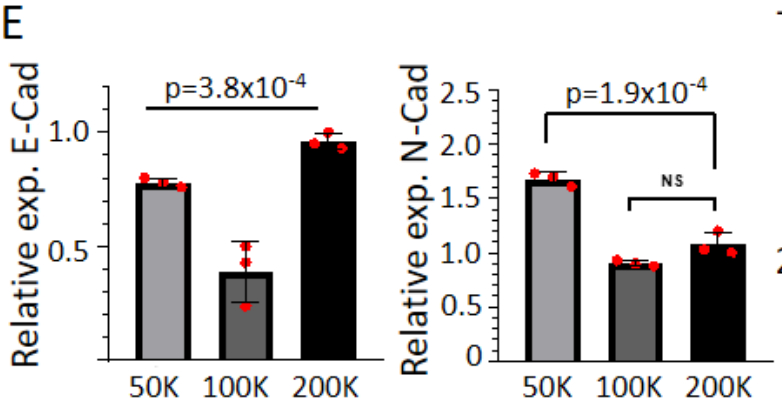
ARTICLE IN PRESS





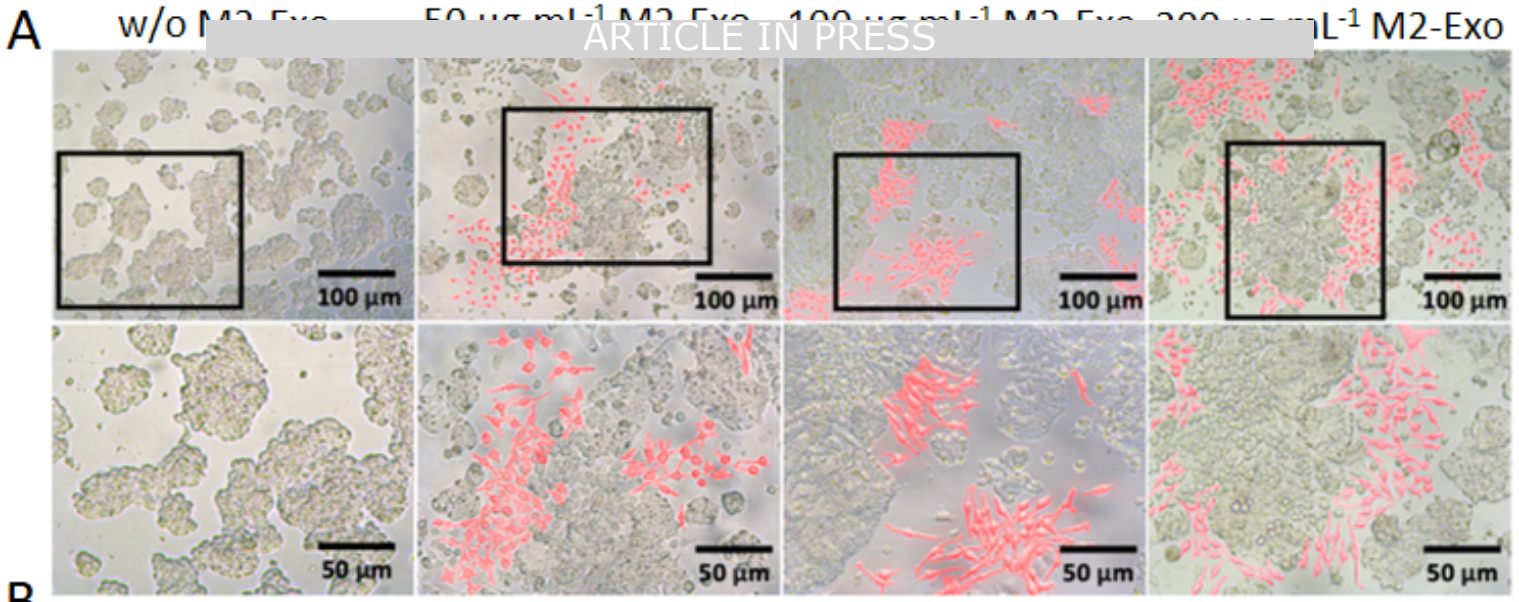


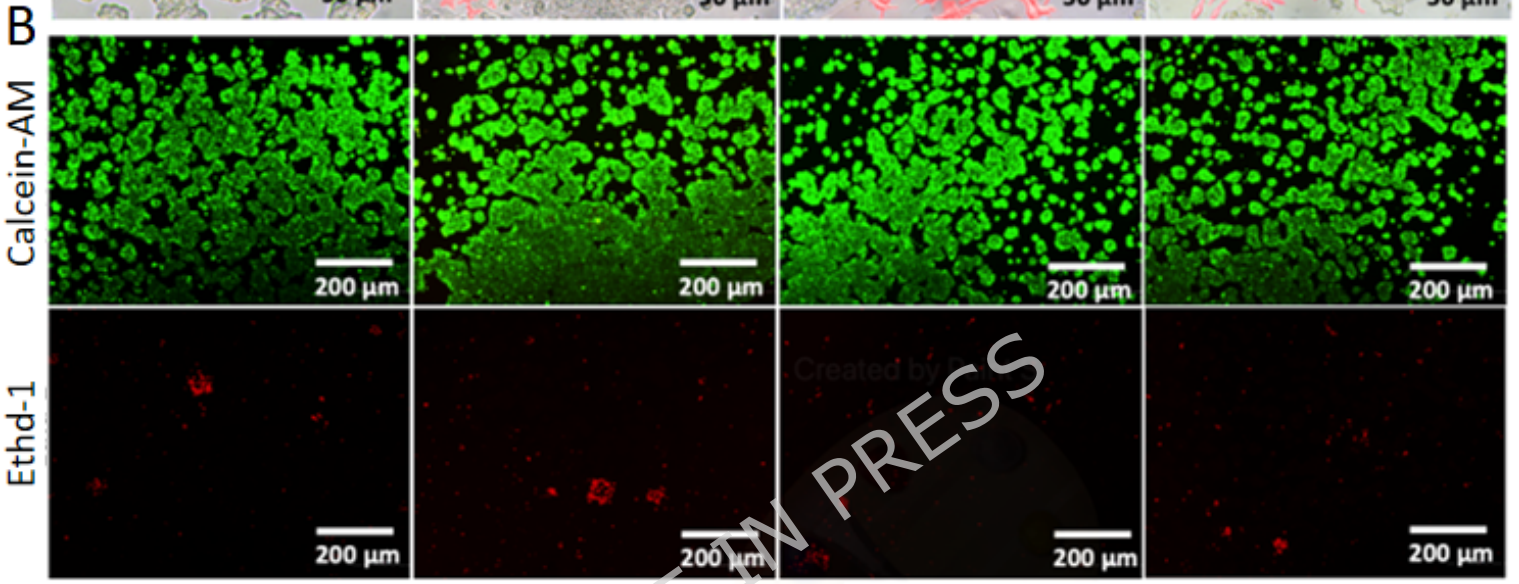


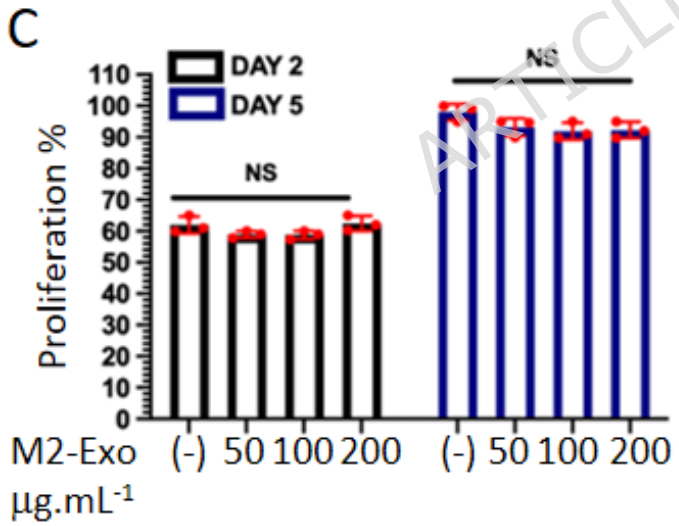


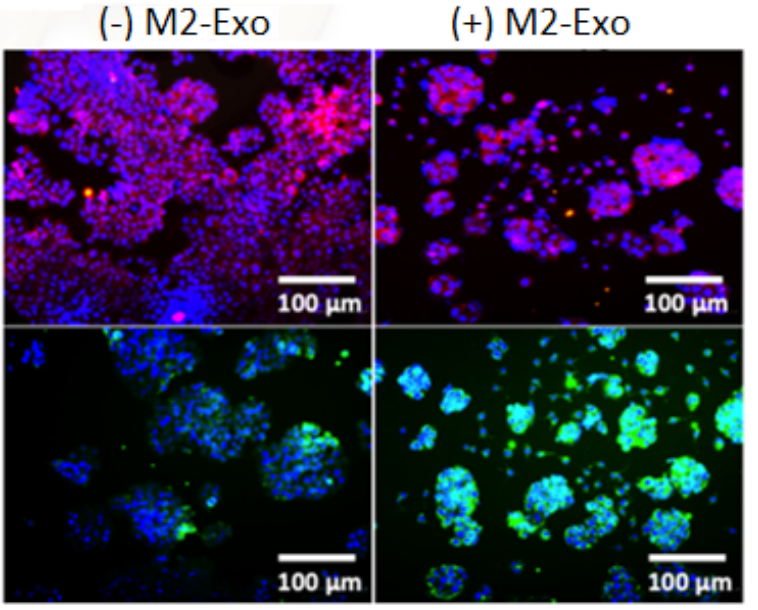
ARTICLE IN PRESS

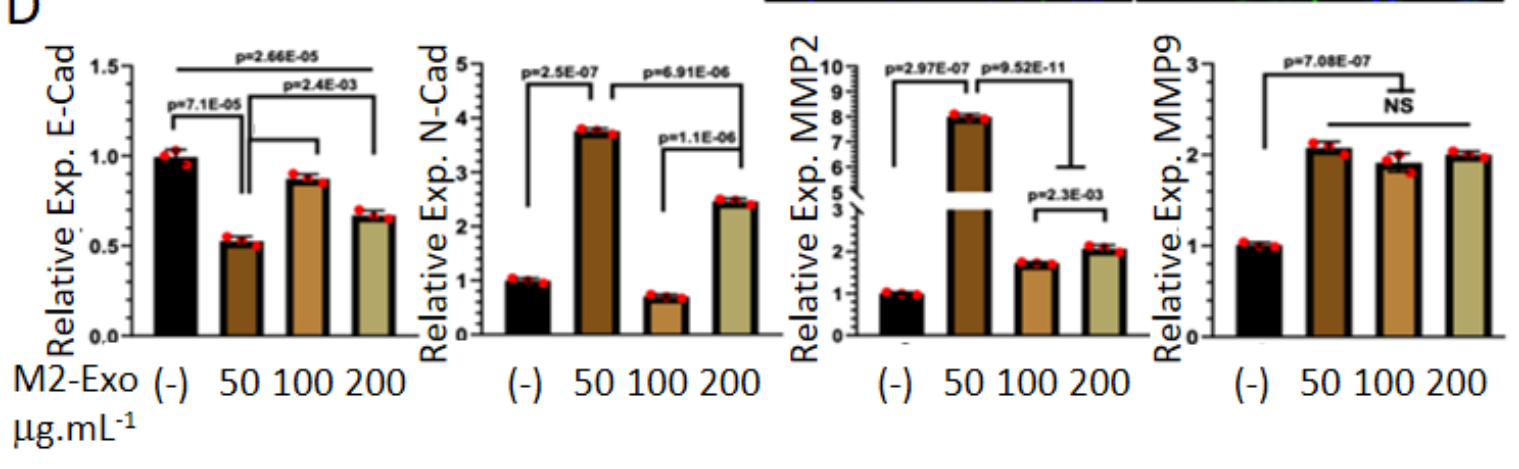
ARTICLE IN PRESS



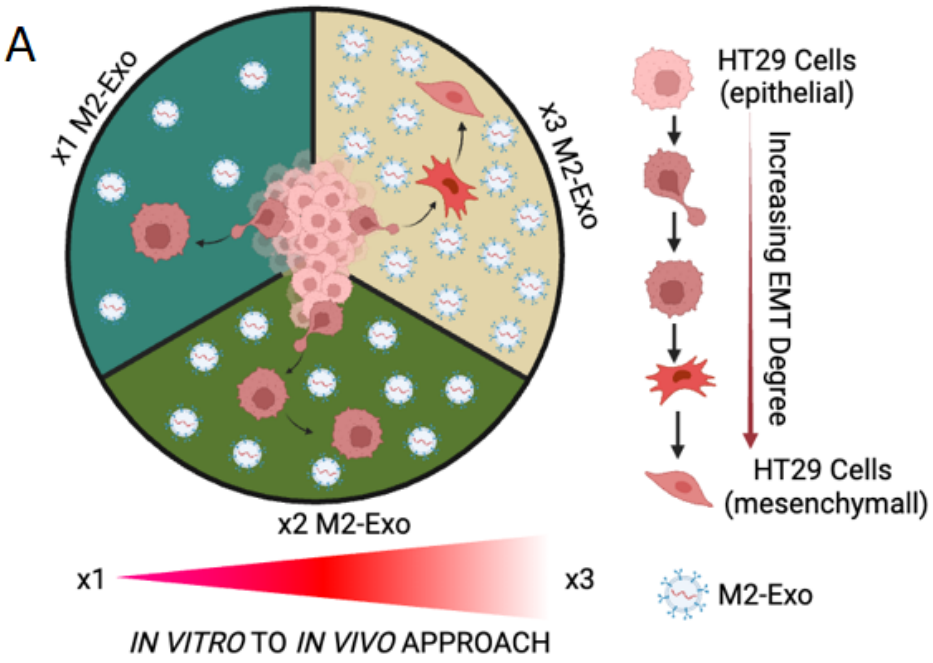


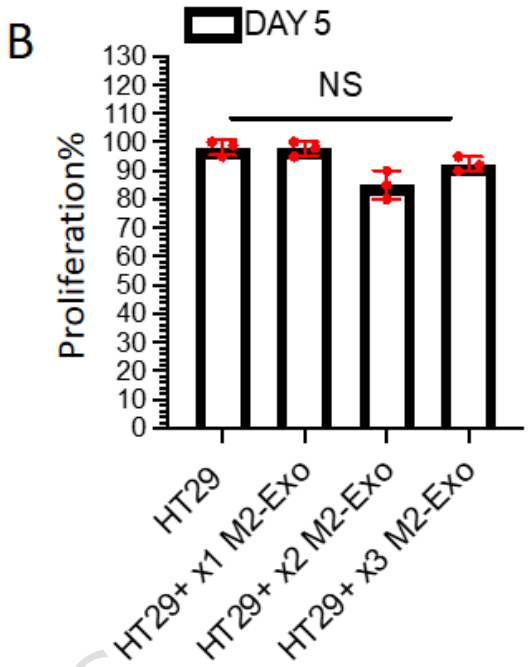


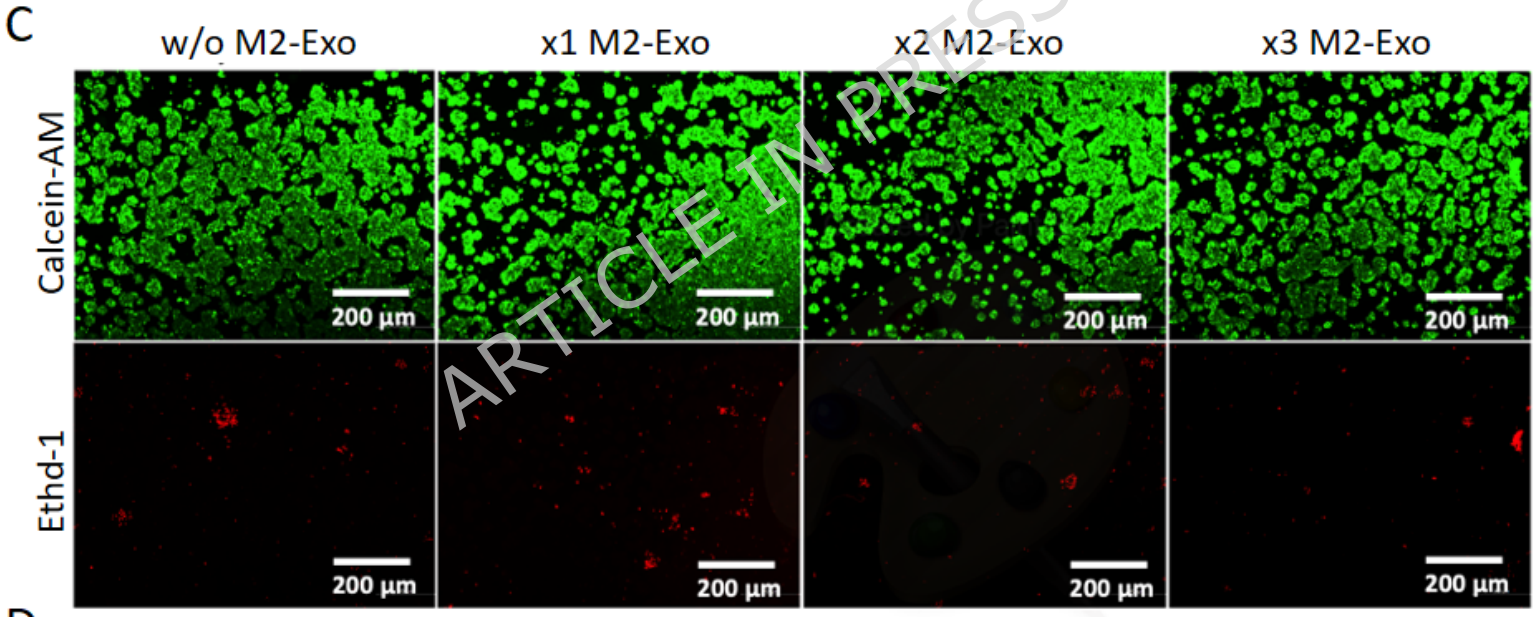


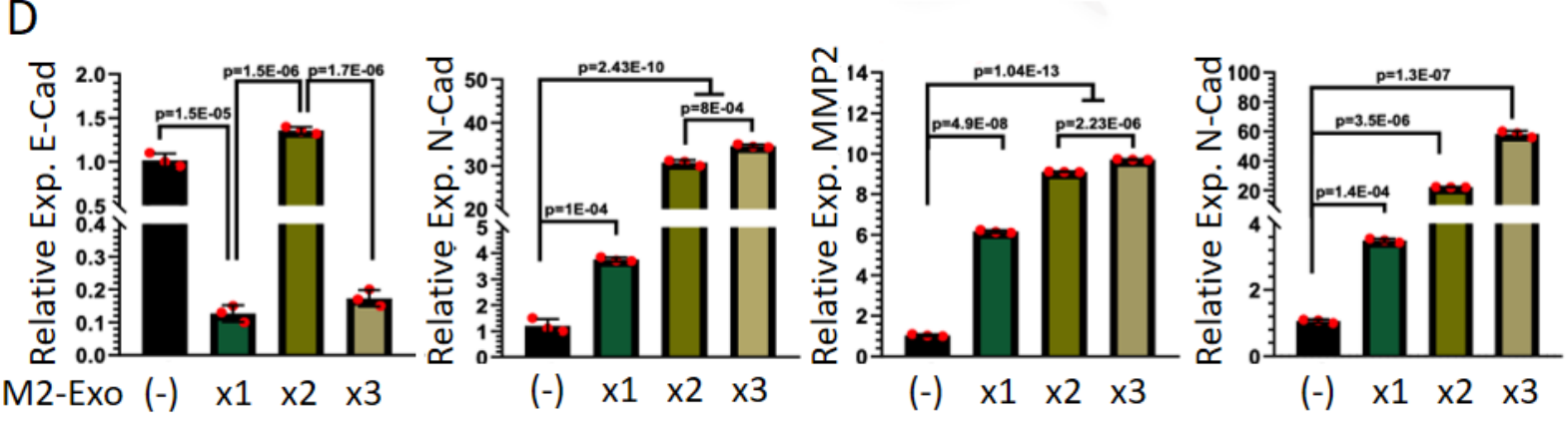


ARTICLE IN PRESS

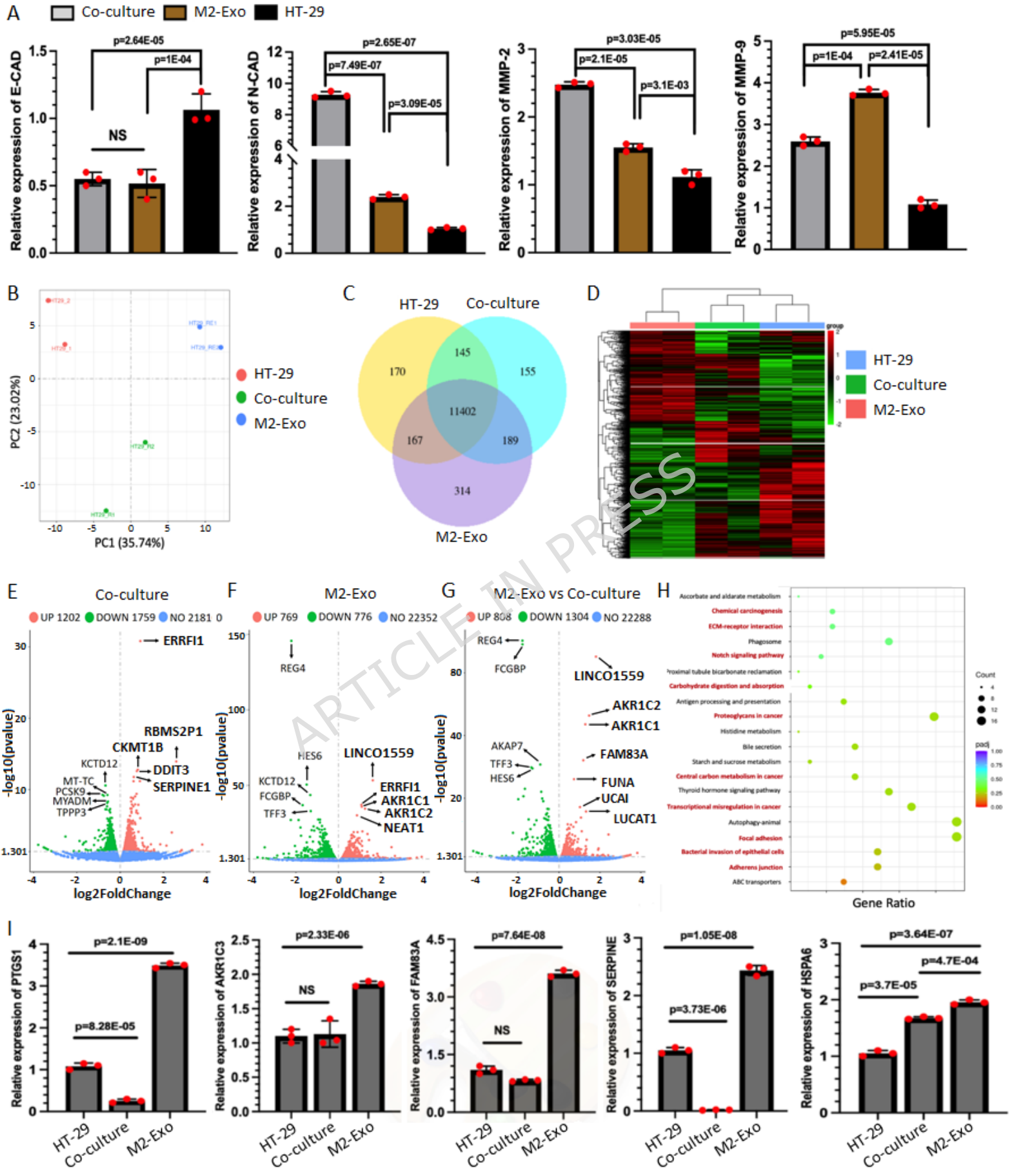




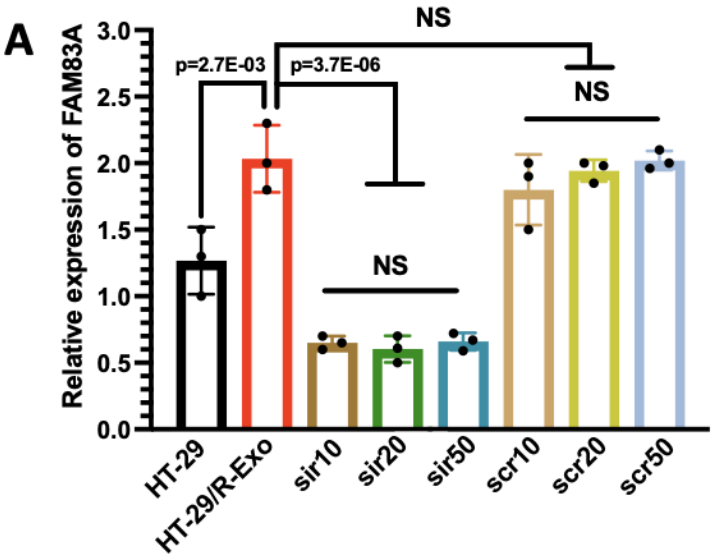


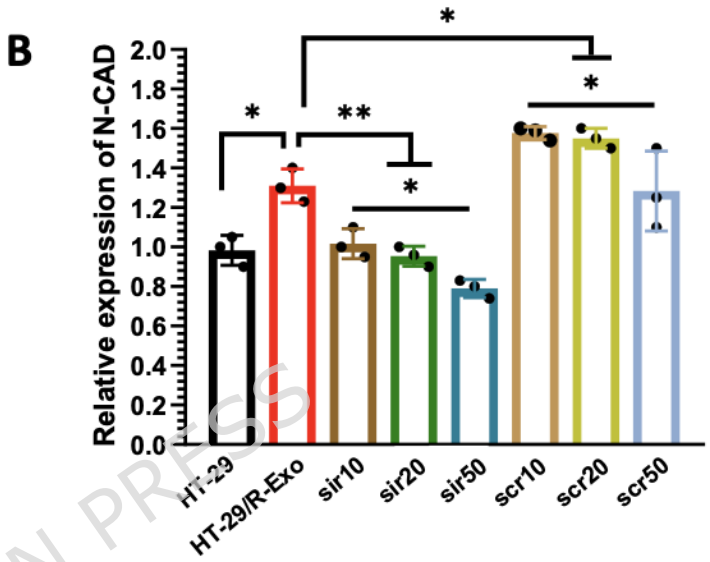


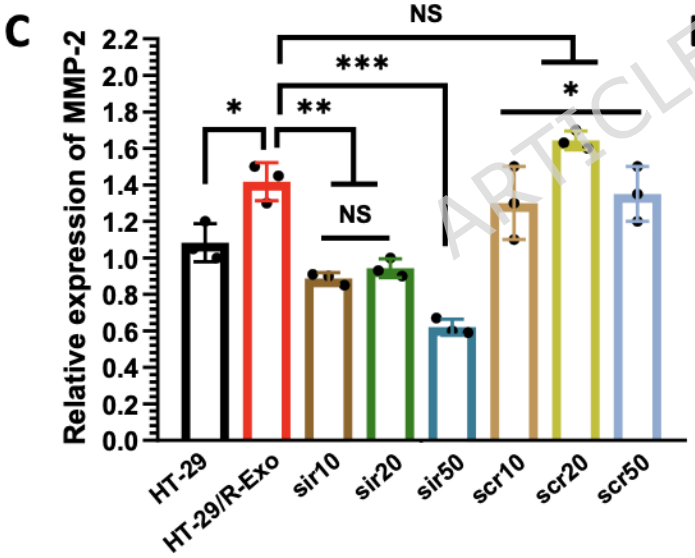
ARTICLE IN PRESS

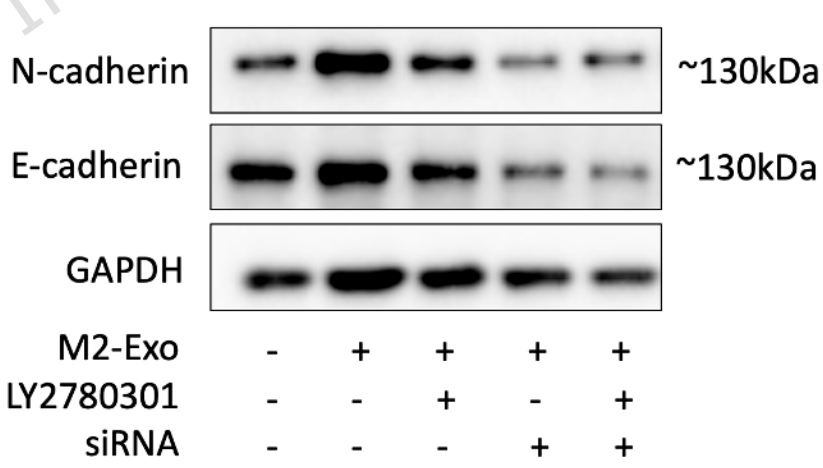


ARTICLE IN PRESS



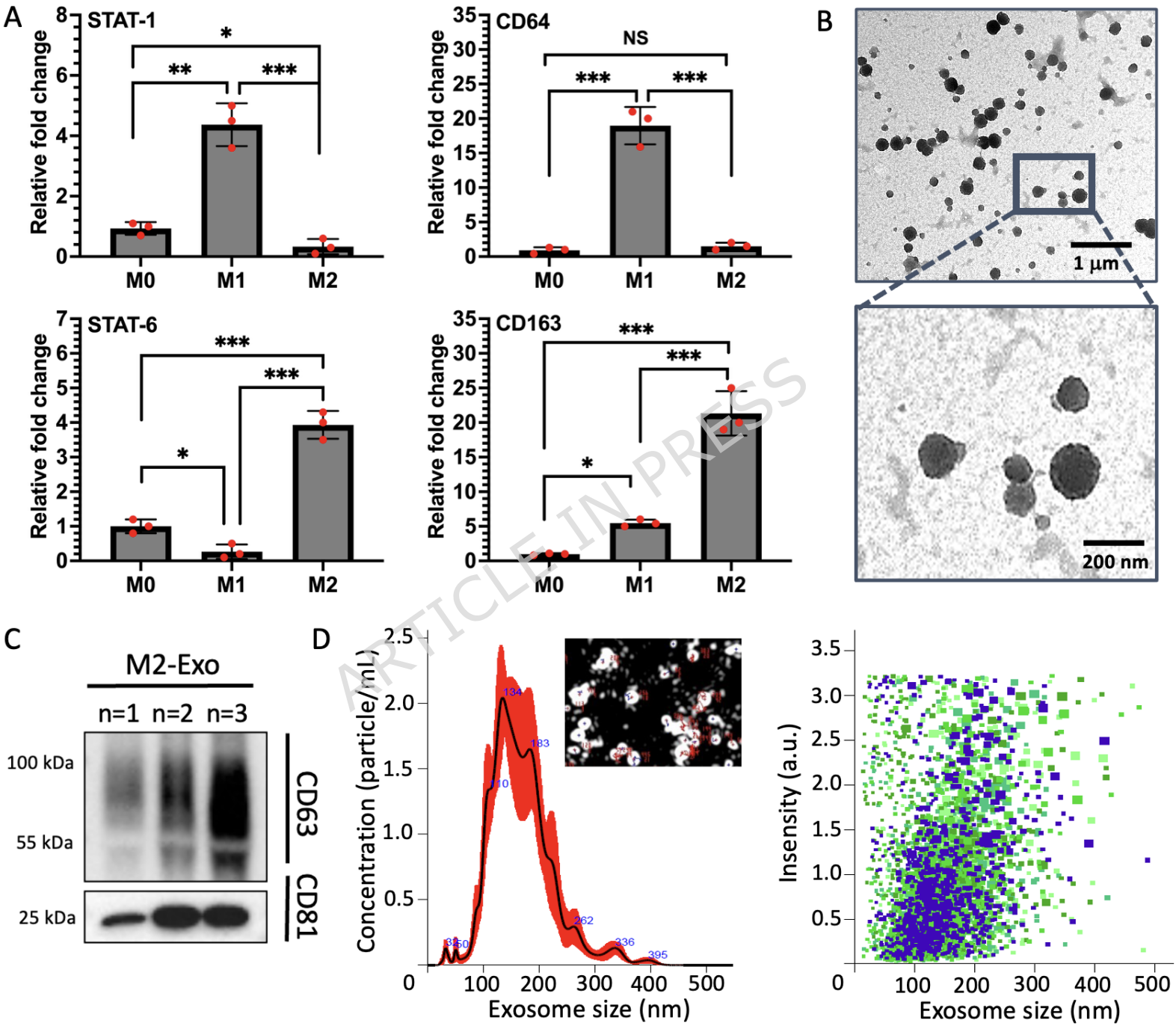






ARTICLE IN PRESS

ARTICLE IN PRESS



ARTICLE IN PRESS